

# Using Point to Set Correlations to Probe the Unjamming Transition

M Mailman<sup>1</sup> and B Chakraborty<sup>2</sup>

<sup>1</sup>Department of Physics, IPST and IREAP, University of Maryland, College Park, Maryland, 20742

<sup>2</sup>Martin Fisher School of Physics, Brandeis University, Waltham, Massachusetts 02454 and

E-mail: mailmm@brandeis.edu, bulbul@brandeis.edu

**Abstract.** We present a detailed analysis of the unjamming transition in 2D frictionless disk packings using a static correlation function that has been widely used to study disordered systems. We show that this point-to-set (PTS) correlation function exhibits a dominant length scale that diverges as the unjamming transition is approached through decompression. In addition, we identify deviations from meanfield predictions, and present detailed analysis of the origin of non-meanfield behavior. A mean-field bulk-surface argument is reviewed. Corrections to this argument are identified, which lead to a change in the functional form of the critical PTS boundary size  $R_0$ . An entropic description of the origin of the correlations is presented, and simple rigidity assumptions are shown to predict the functional form of  $R_0$  as a function of the pressure  $P$ .

PACS numbers: 45.70.-n, 46.65.+g, 64.60.Ej

## 1. Introduction

It is widely believed that unjamming of disk packings is a singular point: as  $P \rightarrow 0$  (or  $\phi \rightarrow \phi_c$ ), a disk packing loses rigidity and ceases to be a solid[1, 2]. What is still up to debate is whether or not this point represents a critical point in the sense of a true thermodynamic phase transition. In critical phenomena, an important signature of a phase transition is a characteristic length scale that emerges from the statistical mechanical system and becomes the system size (diverges in the thermodynamic limit) when the system reaches the critical point. The origin of such a length scale lies in spatial correlations of the statistical variables within individual microstates that become longer ranged as the critical point is approached. As a result, such a length scale is an inherent property of static configurations.

Measures of such a length scale in granular systems have been widely sought after, and with some success. But, what is still missing is an understanding of the correlations that are associated with the relevant length scale in granular systems. We begin by discussing previous studies of the length scale in granular systems, and their interpretation. This previous work includes the study of correlations in velocities and non-affine displacements in unjammed, flowing granular packings under shear[3], as well as force fluctuations which are measured in response to point perturbations in jammed packings[4]. A theoretical framework based on mean-field bulk-surface arguments is discussed, which predicts a growing length scale[5, 6].

In this paper, we expand on the work of [7], where it was shown that a static correlation function exhibits a length scale that diverges in the thermodynamic limit for computer-generated packings of disks in 2D. This ‘‘Point-to-Set’’ correlation function (PTS) is motivated by the Random First Order Transition (RFOT) theory of glasses[8, 9, 10, 11, 12]. We calculate the PTS correlation function in 2D disk packings through the use of the force network ensemble, which has been studied extensively as a model of overcompressed jammed packings[13, 14, 15]. We investigate the origins of this correlation function starting from an entropic formulation of the space of solutions to mechanical equilibrium of the disk packings. Through our analysis of the microscopic nature of the correlations, we gain insight into the unjamming transition, and especially, the deviations from the mean-field predictions.

## 2. The Isostatic Argument

The first indications that there might be a critical point associated with jamming and unjamming of spherical grain packings dates back to discussions of marginal rigidity by Maxwell[16], and has been revisited in for instance [6, 17]. In the limit of hard spheres and an infinite system size in  $d$  dimensions, the number of contacts  $z$  of a packing can be calculated exactly. The hardness leads to a geometric constraint: no two spheres can overlap. Therefore, for any two spheres with diameters  $D_i$  and  $D_j$ , the center-to-center distance between the two spheres  $R_{ij} \geq (D_i + D_j)/2$ . The coordinates

that locate the centers of the spheres act as degrees of freedom, with  $dM$  such degrees of freedom for  $M$  spheres, and the overlap constraints are applied at each contact, of which there are  $M[z]/2$ , if each grain has on average  $[z]$  contacts. The 2 takes into account the double-counting of contacts. In order to satisfy each constraint and still be consistent, the number of degrees of freedom must be greater than or equal to the number of constraints:  $dM \geq M[z]/2$ .

In the case of soft spheres at non-zero pressure, some spheres must overlap. Instead, it is the contact forces that are determined by the constraints imposed by mechanical equilibrium. There are  $M[z]/2$  contact forces, and  $dM$  mechanical equilibrium equations which must be satisfied. Therefore,  $dM \leq M[z]/2$  in order for a packing of soft spheres to be mechanically stable.

In the limit of hard spheres and zero pressure, both inequalities can be satisfied only when both inequalities are equalities:  $dM = M[z]/2$  so that  $[z] = 2d = z_0$ . In particular, for two dimensions the “isostatic” value  $z_0$  is 4.

When grains are soft,  $[z]$  can become greater than  $z_0$  as the packing fraction is increased. With respect to unjamming of soft grains, the observation that there is a minimal value of  $[z]$  below which the pressure of the packing must go to zero and cannot be mechanically stable suggests that the isostatic point  $z_0 = 2d$  might be a critical point, since states with  $[z] > z_0$  are expected to flow to a jammed, mechanically stable fixed point and state with  $[z] < z_0$  to an unjammed, gas-like state. This transition, however, happens out of equilibrium, and an interesting question to ask is whether there is a diverging length scale associated with the isostatic point.

### 3. The Hunt for a Granular Length Scale

#### *Bulk-Surface Argument and the Isostatic Length Scale*

A length scale in overcompressed jammed packings that increases as they are decompressed (pressure  $P \rightarrow 0$ ) is predicted from a bulk-surface argument. Based on counting arguments that date back to Maxwell[16], and more recently discussed in [6, 17], one begins with  $M[z]/2$  force bearing contacts in a subregion of a packing, where  $M$  is the number of grains in the subregion and  $[z]$  is the average number of contacts per grain of the packing. For each of the  $M$  grains, there are  $dM$  equations of mechanical equilibrium (ME) constraining the forces at each of the  $M[z]/2$  contacts (in  $d$  dimensions). As is discussed below, in the limit of very stiff grains, the deformations of two grains in contact are impossible to resolve even though contacts can carry a great deal of force. The only constraints on these contact forces, then, are ME equations, and force laws can be ignored. There are  $M[z]/2 - dM = M\delta z/2$  unconstrained contact force magnitudes, which are taken to be the degrees of freedom, with  $\delta z = [z] - z_0$ . Finally, if one defines a subregion by a set of boundary grains, these grains provide an additional  $A$  constraints from the boundary. Roughly,  $A \propto \sqrt{M}$  in 2D. The number of

grains can be estimated using the definition of the packing fraction:

$$\phi = c \frac{Mr^2}{L^2} \rightarrow M = \frac{\phi}{c} R^2 \quad (1)$$

The unitless length  $R$  is the ratio of size of the subregion  $L$  to the radius  $r$  grains (for our purposes, systems are bidisperse and  $r$  is taken to be the diameter of the smaller grain), and the parameter  $c$  characterizes the polydispersity.

Using 1, the number of excess contact force degrees of freedom  $\delta n$  can be written as a function of  $R$ . In 2D,

$$\delta n_{nom} = \frac{M\delta z}{2} - A = \alpha\phi R^2\delta z - \beta\sqrt{\phi}R \quad (2)$$

where  $\alpha$  and  $\beta$  are constants. This is a nominal expression for  $\delta n$ , hence the subscript “nom,” and will be discussed in more detail in the proceeding sections.

At this point, it's worth contrasting the bulk-surface argument presented here with those found in the literature [5, 6]. In previous constructions of the bulk-surface argument, the boundary of the subregion is said to contribute a set of fixed, “frozen” contact forces, so that the total number of excess contacts  $M\delta z/2$  is *reduced* by  $A$  contacts. This should be contrasted with the above construction, where the boundary term contributes *additional* boundary constraints on the variable contact forces. Near isostaticity, there is no difference between the two constructions, but away from isostaticity, the boundary term in the formulation of [5, 6], when contributing extra frozen contacts, should scale with  $z$ :  $A \propto \sqrt{M}[z]$ , since on average there are more contacts on the boundary if there are more contacts in the packing as a whole.

Frozen contact forces differ from additional constraints due to ME: the former reduce the number of degrees of freedom [5, 6] and are proportional in number to  $[z]$  while the latter serve to further determine the existing contact forces and are proportional in number to  $M$ . An important length scale is determined by  $\delta n_{nom}(R_0) = 0$ . This length scale defines the size of the smallest region within which the mechanical equilibrium equations can be satisfied, and  $R_0 \propto \delta z^{-1}$  if one assumes that the dependence on  $\phi$  is small. In the existing literature [5], this length scale, referred to as the isostatic length scale  $l^*$ , is deduced from a form of the bulk-surface argument that depends on frozen boundary contact forces. There is no difference in the results of the two constructions as  $\delta z \rightarrow 0$ . However, with boundary contact forces frozen,  $l^* \sim \frac{[z]}{\delta z}$ , and can differ significantly from  $R_0$  at large overcompressions. In [4] the isostatic length scale is measured indirectly through the response to a point-force perturbation to mechanically stable overcompressed packings, and is shown to scale as  $1/\delta z$ . In later sections, it will be made clear why a bulk-surface argument of the form 2 is preferable in the context of the PTS correlation.

The vibrational spectrum of granular packings as defined by the dynamical matrix provides more insight into the nature of unjamming. The excess degrees of freedom  $\delta z$  can be related to the pressure of the packing through the vibrational density of states [5, 18]. A critical frequency  $\omega^*$  is associated with the highest energy debye-like

mode of a marginally stable packing. Anomalous modes (modes whose density of states are roughly independent of the frequency) appear at energies higher than  $\omega^{*2}$ , and this energy difference is proportional to  $-P$ . So, the energy change due to an imposed pressure  $P$  is  $\Delta E \leq \omega^{*2} - AP$  and the critical frequency is  $\omega^* \propto P^{1/2}$ . To relate  $\omega^*$  to the contact number, one must look at the characteristic size of the anomalous modes. It turns out that anomalous modes with  $\omega \geq \omega^*$  are quasi-localized with localization length  $\geq R_0$ [19]. Assuming a linear dispersion relation  $\omega \propto ck$ , the critical frequency is:  $\omega^* \propto \frac{1}{R_0} \propto \delta z$ , and therefore,  $\delta z \propto P^{1/2}$ [20, 21].

It should be noted that the validity of the dynamical matrix approach to deriving the vibrational spectrum has been recently called into question[22]. Numerical studies show that in the limit of infinite system sizes, arbitrarily small perturbation amplitudes lead to contact breaking, and mixing of the eigenmodes of the dynamical matrix[22]. This result calls into question any analysis of response of jammed packings based on the vibrational density of states. While the result  $\delta z \propto P^{1/2}$  is well established in simulations (we have verified that our numerics reproduce this result), the justification of this relationship relies on the existence of anomalous modes in the vibrational spectrum. Furthermore, the explanation that the length scale measured in collective response is associated with the extent of such anomalous modes becomes questionable, further motivating our choice to look for a static measure of a correlation length.

There are two aspects to the bulk-surface argument which are mean-field in nature. The first is the relation between  $P$  and  $\delta z$ . In principle,  $\Delta E$  should depend on factors which contain the force vector orientations, but it is assumed that these vectors are randomly distributed in the packing so that their effects on  $\Delta E$  average to a constant. If, on the other hand, the local configuration of force vectors depended heavily on the orientations of nearby force vectors, as one might expect for instance simply because of the overlap constraints, this might not be a reasonable assumption. It turns out that at least for isotropically compressed packings, the packing geometry is sufficiently disordered that this assumption is sound[5].

The second mean-field assumption is built into the counting that goes into the bulk-surface argument. The assumption that the number of excess force degrees of freedom is given by the difference between the number of force variables and the number of ME equations requires that these equations are all independent, since a linear system has a number of undetermined variables equal to the difference between the total number of variables and the number of *independent* equations. As will be detailed in the sections below, this assumption does fail significantly as  $P \rightarrow 0$ .

### *Stress Correlations*

The work of [3] on transverse grain displacement correlations in simulations of 2D disk packings under quasistatic shear strain reports a growing length scale for packing fractions below  $\phi_J$ . Interestingly, they find no evidence for a growing length scale as  $\phi_J$  is approached from above. These results are consistent with continuum elastic

theory [23] which shows that shear-strained packings can be thought of as random local forces applied to a homogeneous elastic sheet. Because of this homogeneity, the system size becomes the only relevant length scale of the system. Furthermore, in [24] a field-theoretic calculation of pressure fluctuation correlations for both isotropically compressed and sheared systems shows that such correlations exhibit a power-law behavior, with the only length scale emerging as the grain size, independent of the pressure.

At this point, it would seem that (2-point) stress correlations do not exhibit a growing length scale. Neither do displacement correlations, even though force fluctuations seem to scale with the isostatic length scale  $l^*$ . The latter requires one to consider the response to a point perturbation, and unlike systems in thermal equilibrium, the relation between response and correlations is not established in jamming systems. The question of whether there is a static correlation function that can be identified with the unjamming transition is, therefore, still wide open.

The importance of probing a static correlation function can be understood from contrasting the results from the non-equilibrium unjamming transition to that of, say, a simple Ising model: for a large enough system, a single spin configuration of the magnet equilibrated at some temperature  $T$  will exhibit a spin-spin correlation length that grows as  $T_c$  is approached. One does not have to consider properties of the dynamics which brings one spin configuration into another. If the unjamming transition is to be thought of as a critical point and not a kinetic freezing transition[25], a static correlation function must show a diverging length scale. In section 4 a new type of correlation function is discussed, which is specifically designed to overcome the added complexity of amorphous systems where critical behavior is still to be expected.

#### 4. Point-to-Set Correlations

In the physics of the glass transition, the question of a static correlation function associated with the arrest of dynamics and the onset of the glassy state is also very important, and has been investigated extensively[10]. There has been speculation that the jamming transition is the zero temperature limit of a glass transition driven by compression or shear [1]. Regardless, in both glassy and granular systems there exist metastable states which characterize the statistical mechanics of the glassy or jammed phases [26], and ideas from the glass literature can be used to probe the existence of a growing static length scale associated with unjamming.

In the Random First Order Transition (RFOT) theory of the glass transition, a correlation function is defined[8, 10], which can probe growing amorphous order. In phase transitions characterized by a well-defined order parameter, a 2-point correlation function is sufficient to distinguish between the disordered and ordered state[27]. However, pre-existing knowledge of the structure of the ordered state is built into the definition of the two point correlation function. A simple example demonstrating this is frustrated magnets, where the 2-point spin-spin correlation function fails to clearly

identify the correlations. Instead, one engineers a correlation function which is sensitive to an “ordered state” of staggered spins. This correlation function is constructed with *a priori* knowledge of the ordered state. For an amorphous system, where the free energy landscape can become quite complex, with minima corresponding to different configurations of the particles, no such *a priori* knowledge exists.

Without an intuition for the relevant symmetry needed to describe the jammed or glassy phase to motivate the construction of a correlation function, one instead begins with the “definition” of a thermodynamic second order phase transition[9]: the influence of boundary conditions on the bulk of the system grows as the critical point is approached. Imagine that an Ising magnet is equilibrated at some  $T$  and used to define a boundary condition of spins that are characteristic of that temperature. Then a configuration of spins of size  $R$  is allowed to re-equilibrate with respect to that particular boundary condition. If  $R < \xi(T)$ , the resulting spin configuration will not change much from that of the original equilibrated magnet. However, if  $R > \xi(T)$  then the configuration of spins that is equilibrated with respect to the boundary conditions acts essentially as a free set of spins, insensitive to the boundary conditions, and can re-equilibrate to a very different configuration. An appropriately defined overlap of the equilibrated magnet and the magnet with respect to the boundary conditions captures the relevant correlations and exhibits the diverging length scale  $\xi(T)$ . Such a correlation function is known as the Point-to-Set (PTS) correlation function[12], since it captures the correlations of a single degree of freedom such as a spin with a set of boundary degrees of freedom that are fixed as boundary conditions.

The advantage of this correlation function over typical 2-point correlation function is that it generalizes easily to amorphous systems where the degrees of freedom can be more complicated but the boundaries are still easily defined. For instance, in [12] the PTS correlation function for the p-spin system on a Bethe lattice is calculated exactly and shown to exhibit a growing length scale as the critical temperature is approached, even though the spin configurations of such systems are amorphous. In a more realistic Lennard-Jones glass forming liquid[11], a PTS correlation function is shown to exhibit correlations that persist for larger values of  $R$  as the temperature is decreased.

With the PTS correlation function, there is no general framework for the definition of the overlap. It appears to be very system specific. For instance, in [11] the overlap of the “reference state” (the equilibrated configuration of particles) with the “pinned state” (equilibrated with respect to a fixed boundary) is defined as the product of the thermally averaged occupation number of discrete cells which are used to discretize space.

Roughly speaking, what we learn from these examples is that a PTS correlation function should have the property that it compares a typical “reference” configuration of the system to a “pinned” configuration of the system which is typical given a particular set of boundary conditions, themselves derived from the reference configuration. Some overlap must be defined that captures how similar the reference and pinned states are. The dependence on distance in the correlation function always results from the size of

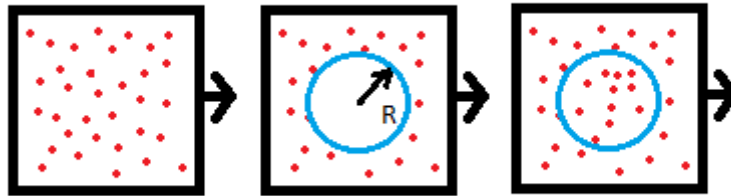


**Figure 1.** In general, the protocol for calculating a PTS correlation function involves finding an equilibrated state of the system (left, with red dots representing degrees of freedom). Then, a boundary of size  $R$  is defined, where degrees of freedom outside are kept fixed (middle) and inside are allowed to continue to fluctuate, but with respect to the boundary conditions imposed by the fixed degrees of freedom.

the bounded region of the pinned state (figure 1).

## 5. The Force Network Ensemble and a Granular PTS

### *Definition of the Force Network Ensemble*

The Force Network Ensemble (FNE) has been studied extensively as a statistical mechanical model of granular matter[14]. While there are several variations on the model studied in the literature[28, 15, 13], the key assumption made when developing the FNE is that when grains are sufficiently rigid, infinitesimally small deformations of grains (or, simply deformations that are too small to observe experimentally) lead to significant fluctuations in the contact forces. With this assumption, the force law coupling grain deformations to forces is no longer relevant. For a given fixed configuration of mechanically stable grains (referred to here as an MS), the contact forces can take on any positive values that do not violate the constraints of mechanical equilibrium (ME). When the grains are frictionless, the forces  $\vec{f}_{ij}$  always lie along the vector normal to the point of contact  $\hat{r}_{ij}$ , which in the case of disks is the center-to-center separation vector between grain  $i$  and its neighbor  $j$ . The ME constraints are linear in the contact force magnitude, and are expressed as[29]:

$$\sum_{j=1}^{z_i} \hat{r}_{ij} f_{ij} = 0 \quad (3)$$

In addition, there are generally global constraints from the force moment-tensor of  $M$  grains

$$\sigma_{\alpha\beta} = \sum_{i=1}^M \sum_{j>i}^M \frac{f_{ij} r_{ij}^{\alpha} r_{ij}^{\beta}}{r_{ij}} \quad (4)$$



(for  $\alpha, \beta = x, y$  in 2D) on the force networks, which are linear in the contact forces. These global constraints are inhomogeneous since the stress of a jammed packing is greater than zero. The linear system of equations is expressed as a matrix equation

$$A\vec{f} = \vec{b} \quad (5)$$

The matrix  $A$  is made up of the geometric information of the MS. In particular, it contains the components of  $\hat{r}_{ij}$ . The vector  $\vec{f}$  is a list of contact force magnitudes  $N$  long, where  $N$  is the total number of contacts for the MS. The vector  $\vec{f}$  represents a particular force *network* that satisfies ME for a given MS, and should not be confused with a force vector  $\vec{f}_{ij}$  that is applied to a particular grain. The vector  $\vec{b}$  is a list of length  $2M + 3$  (in 2D) that contains the values of the constraints. Entries which correspond to force balance equations are zero, while the entries corresponding to components of the stress tensor are non-zero constants:  $\vec{b} = (0, 0 \dots \sigma_{xx}, \sigma_{xy}, \sigma_{yy})$ .

The matrix  $A$  of the linear system in Eq. 5 is rectangular with dimensions  $2M + 3$  by  $N$  in 2D. A packing with periodic boundary conditions will result in two more constraints on the contact forces in 2D[14]. The istostatic argument of section 2 is easily expressed in terms of the shape of  $A$ : assuming that the equations of ME are all *independent* (an assumption that will be discussed further in the proceeding sections) the packing is isostatic, and hence the linear system 5 is precisely *determined*, if  $A$  is square. If  $A$  is rectangular with more rows than columns, the packing is hypostatic, and therefore Eq.5 *overdetermined*, and if  $A$  is rectangular with more columns than rows, the packing is hyperstatic and therefore Eq.5 is *underdetermined*. For the case where Eq.5 is underdetermined, there is an infinite set of force networks  $\{\vec{f}\}$  that satisfy ME for the given MS. This set makes up a force network ensemble for the given MS, referred to as the MS-FNE. It's important to notice that two MS-FNE's are not interchangeable; a set of force networks for a given geometry is not valid for any other geometry.

Sampling force networks for an amorphous geometry requires solving Eq.5. When the linear system is underdetermined, the matrix  $A$  has a nullity greater than zero, and so the solutions of  $A\vec{f} = \vec{0}$  are spanned by null space of dimension  $\delta z$  (when  $A$  is a full rank matrix). The singular value decomposition (SVD) of  $A$  results in the basis  $\{\hat{g}\}$  of the null space of  $A$ . Since Eq.5 is inhomogeneous,  $\{\hat{g}\}$  are not solutions to Eq.5. Actually,  $\{\hat{g}\}$  are solutions at exactly zero pressure, which requires each basis vector to have both positive and negative elements, violating the positivity constraint. The homogeneous solutions  $\{\hat{g}\}$  must be added to a particular solution  $\vec{f}_0$  which satisfies ME for the given MS and which satisfies the inhomogeneous constraints, including the components of the stress tensor. A good choice of  $\vec{f}_0$  is easily found by applying a force law, for instance linear spring interactions which are used throughout this work, to construct a given MS and then extract a force network from the geometry. In summary, for all  $\{\hat{g}\}$  such that  $A\hat{g} = 0$ , there is a solution  $\vec{f} = \vec{f}_0 + c\hat{g}$  to Eq.5 for an amplitude  $c$ .

A method for sampling force networks for amorphous geometries then amounts to finding a particular MS using any packing protocol, solving for the null space of  $A$  using numerical SVD routines, and choosing amplitudes  $c$  at random to construct new force

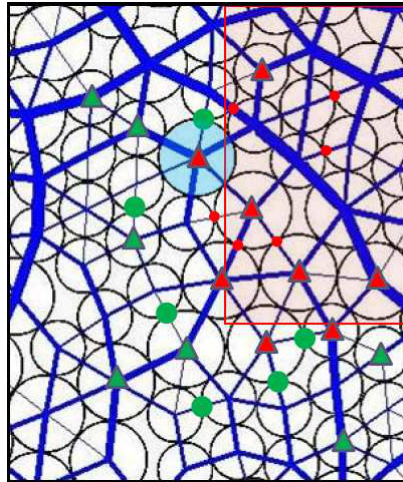


**Figure 2.** A sample disk packing with a boundary drawn in red, illustrating the effects of the boundary on  $A(R)$ . Red triangles identify grains which contribute ME equations to  $A(R) \vec{f}(R) = \vec{b}(R)$ , and red dots are variable contact forces. Green circles, on the other hand, are not considered variable contact forces, and green triangles identify grains which do not contribute extra constraints to the linear system. The blue grain is an example of a grain that plays the special role of contributing ME equations to the linear system, but which only has two fluctuating contact forces (the contact forces that cross the boundary). The rule is that if the center of a grain lies within the boundary, all of its contact forces will be variables.

networks  $\vec{f}$  from  $\vec{f}_0$  and  $\{\hat{g}\}$ . As with the wheel move[28], which can be shown to be a particular null vector of the  $A$  corresponding to the triangular lattice, the positivity constraint must be obeyed, and so any  $\vec{f} = \vec{f}_0 + c\hat{g}$  must be rejected if the resulting  $\vec{f}$  has any negative elements. This approach to sampling the FNE was first developed in [15].

### *Application of a Frozen Boundary*

It is not yet clear how to construct the PTS correlation function for granular systems. A procedure analogous to that of LJ glass formers might be to remove grains from a subregion of a packing and replace them with a configuration of grains that originates from another packing, and energy minimize to find the new mechanically stable packing while keeping the boundary grains fixed. This approach presents several issues. First, without thermal fluctuations it is not clear that the final state is in equilibrium. There are large energies associated with grain overlaps at the boundary. More fundamental though is the problem of defining the correlation function. Since relevant variables such as local stresses and forces are generally defined with respect to the individual grains or contacts, and number of grains and contacts can vary between subregions (as well as their locations), there is no clearly defined overlap. With the added machinery of the MS-FNE, though, a well-defined correlation function presents itself. For a given MS, we define a PTS correlation function probes the correlations between valid force networks

that make up the FNE. The PTS correlation function  $C$  is then well defined as the inner product of any valid force network  $\vec{f}$  with the initial force network  $\vec{f}_0$ , normalized by the magnitudes of the force networks to guarantee that  $C$  is never greater than 1:  $C = \hat{f}_0 \cdot \hat{f}$ . But, this correlation function still is not a function of a boundary size  $R$ . Fortunately, the FNE allows for the *net* force on a particular grain to be fixed to a value other than zero through the addition of inhomogeneous constraints to  $A$ . First, a boundary of size  $R$  is defined on a subregion of the packing. For the work discussed here, the boundaries are always square to match the symmetry of the simulation box. Grains that are on the interior of the boundary are considered in force equilibrium. They contribute ME equations to  $A$  which are homogeneous. Grains on the boundary, on the other hand, contribute inhomogeneous constraints to  $A$ ; the neighbors of those boundary grains that are exterior to the boundary exert a fixed net force on the boundary grain. These exterior grains do not themselves contribute ME equations to  $A$ . All of the contact forces which are associated with grains that have centers which lie interior to the boundary are considered “free” and are allowed to fluctuate. Contacts outside of the boundary are not allowed to fluctuate and do not contribute to the columns of  $A$  (see figure 2). The matrix  $A$  now depends on the boundary size  $R$ . As  $R$  increases, more grains and contact forces fall into the interior of the boundary, and so the dimensions of  $A$  grow. In addition, the vector  $\vec{b}$ , which now depends on  $R$  as well, will have entries corresponding to the fixed effective external forces being exerted on the boundary grains from their exterior neighbors. The matrix equation  $A(R)\vec{f}(R) = \vec{b}(R)$  must now be solved using the approach outlined for sampling the MS-FNE. A well defined PTS correlation function can now be constructed so that it is dependent on the size of the boundary:  $C(R) = \hat{f}_0 \cdot \hat{f}(R)$ .

As was discussed in section 3, the bulk-surface argument is chosen to have a boundary term which corresponds to the number of grains contributing ME equations to the constraints on the contact forces, rather than a count of the number of “frozen” contact forces. Here, a bulk-surface argument based on frozen contact forces would be an error. There is no way of fixing the contact forces at the boundary. Only *net forces* on each boundary grain can be fixed. Fixing contact forces would involve fixing elements of  $\vec{f}$ , which cannot be done given the approach to sampling the FNE described here, since there is no control over the particular values that the members of  $\{\hat{g}\}$  can take when computing the SVD of  $A$ .

The correlation function  $C(R)$  is computed by averaging over many force networks  $\vec{f}(R)$  and, once a sufficient sampling of the FNE has been completed, the sampling is repeated for many MS. Averages over the FNE are identified with  $\langle \rangle$  brackets, and quantities that are averaged over the set of MS are identified with  $\langle \rangle_g$  brackets. Also, the size of the bounding box  $R$  can be varied and the process repeated for different values of  $R$ . The only relevant microscopic scale is the grain diameter  $D$ , so in practice the parameter that is controlled is the scaled boundary size  $R = R/D$ . In the end, the correlation function studied here for disk packings is  $\langle \langle C(R) \rangle \rangle_g = \left\langle \left\langle \hat{f}_0 \cdot \hat{f}(R) \right\rangle \right\rangle_g$ .

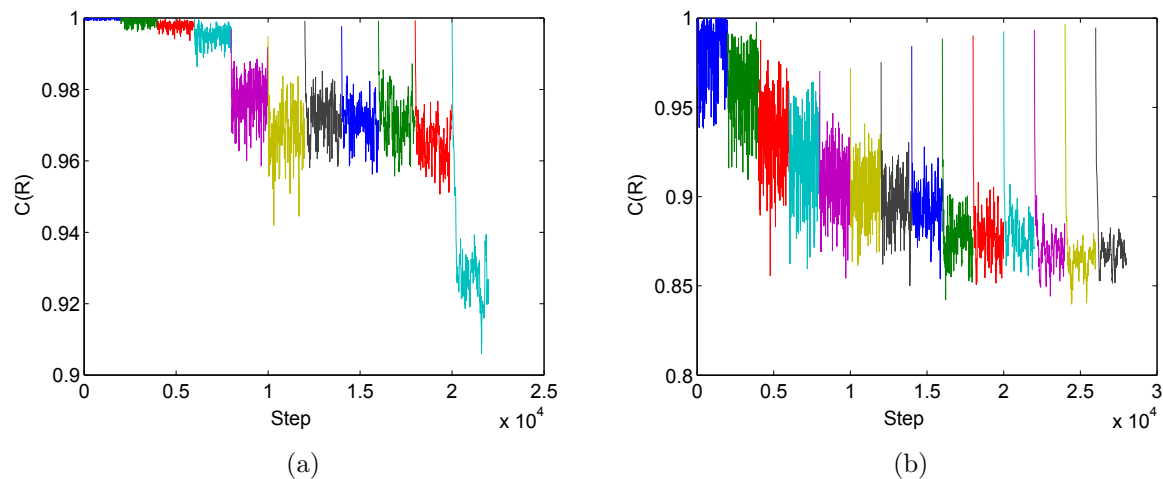


**Figure 3.** (a) A single trajectory for  $C(R)$  at an overcompression of  $\delta\phi = 0.01$ . Changes in the color represent an increase in  $R$ , after which the sampling is allowed to re-equilibrate to the new boundary conditions. The changes in  $C(R)$  with  $R$  are abrupt, but for a particular value of  $R$ ,  $C(R)$  quickly decays and then fluctuates about an equilibrium value. (b) The same, but for  $\delta\phi = 0.1$ .

## 6. Numerical Results for PTS

### *The Correlation Function $C(R)$*

For systems of disk packings ranging from 30 to 900 grains in 2D, bidisperse with one third of the grains 1.4 times larger than the other two thirds [30, 31],  $\langle\langle C(R) \rangle\rangle_g$  has been measured. The MS averaging is done over 40 packings. The FNE averaging is done over  $10^6$  different force networks. Force networks are found by creating a high dimensional random walk in the null space of solutions to  $A(R)\vec{f}(R) = \vec{b}(R)$ , with a random step size chosen from a uniform distribution on an interval  $[-c, c]$  where  $c$  is some fixed constant. The random walk always begins from the initial force network  $\vec{f}_0$ . In practice, a value of  $c = 0.05$  is found to keep the success rate of the sampling high (as few steps as possible violate the positivity constraint) while quickly moving away from the initial force network  $\vec{f}_0$  for a wide range of overcompressions and system sizes. For the largest system size, figure 3 illustrates the trajectory of the random walk by calculating  $C(R) = \hat{f}_0 \cdot \hat{f}_i(R)$  for each random walk step  $i$ . When  $R$  is changed, value of  $C(R) = \hat{f}_0 \cdot \hat{f}_i(R)$  quickly drops and fluctuates around some value for that  $R$ . This acts as a direct verification in terms of the correlation function that the force network sampling has been allowed enough time to “equilibrate,” and that the correlation function is measuring equilibrium properties of the FNE.

The results for  $\langle\langle C(R) \rangle\rangle_g$  for the largest system size of 900 grains is shown in [7]. At small  $R$ , the correlation function is nearly 1, and at some value of  $R$  it begins to decay. As will be discussed below, the tail is a power law in  $R$ , and does not produce a length scale. However, the crossover value of  $R$  where the correlation function begins to

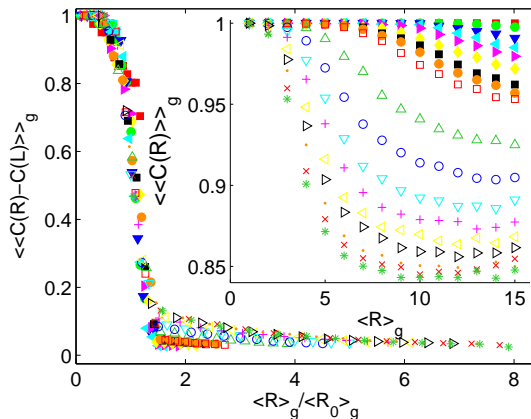


**Figure 4.** The connected correlation function for  $M = 900$ . (Inset) The measured PTS correlation function, with different colors and symbols corresponding to different  $\delta\phi$ . Open symbols range from 0.01 to 0.1 (in increments of 0.01) and filled symbols range from 0.001 to 0.008 (increments of 0.001). The highest  $\delta\phi$ , and hence the highest pressures, correspond to the curves in the inset which decay to the lowest values.

decay does exhibit the characteristics of a critical length scale. This crossover value is referred to here as  $R_0$  because of its relationship to the  $R_0$  of the bulk-surface argument, which will be discussed in more detail below.

In addition,  $\langle\langle C(R) \rangle\rangle_g$  appears to asymptote to some value greater than zero for large  $R$ . Subtracting off this asymptotic value  $q_0 = C(R = L/d)$ , for linear system size  $L$ , one can define a connected correlation function  $\langle\langle C(R) - q_0 \rangle\rangle_g$ . When  $R$  is scaled by  $R_0$ , the connected correlation function collapses onto a master curve that decays rapidly to zero, a functional form which RFOT theory predicts for the PTS correlation function [8, 32].

#### *Deviation from the Mean-Field Exponent: Finite Size Scaling*

Since  $\delta n(R < R_0) = 0$ , there is no null space of  $A(R)$ . The correlation function  $C(R)$  for  $R < R_0$  is identically 1 since  $C(R < R_0) = \hat{f}_0 \cdot \hat{f}_0 = 1$ . The length scale is extracted from the numerics by identifying that value of  $R$  at which  $\delta n(R)$  is first greater than zero (or the value of  $R$  at which  $C(R)$  is less than 1). As a function of  $\langle P \rangle_g$ , the geometry-averaged critical length  $\langle R_0 \rangle_g$  fits a power law. A linear fit of  $\ln(\langle R_0 \rangle_g)$  as function of  $\ln(\langle P \rangle_g)$  establishes an exponent of  $\nu = 0.461 \pm 0.012$  with a 95% confidence interval for the largest (900 grain) packings (figure 5). The lowest overcompression,  $\delta\phi = 0.001$ , is left out of the fit because nearly all of the geometries have  $R_0 = L$ . The inclusion of  $\delta\phi = 0.001$  changes the exponent to  $\nu = 0.45 \pm 0.015$ . Either way, while the exponent is near the mean-field value of 0.5, the difference is significant considering the confidence bounds.

The exponent is verified using finite size scaling. Since all of the numerical results are done at finite system sizes, the exponent that is observed in power law fits may be

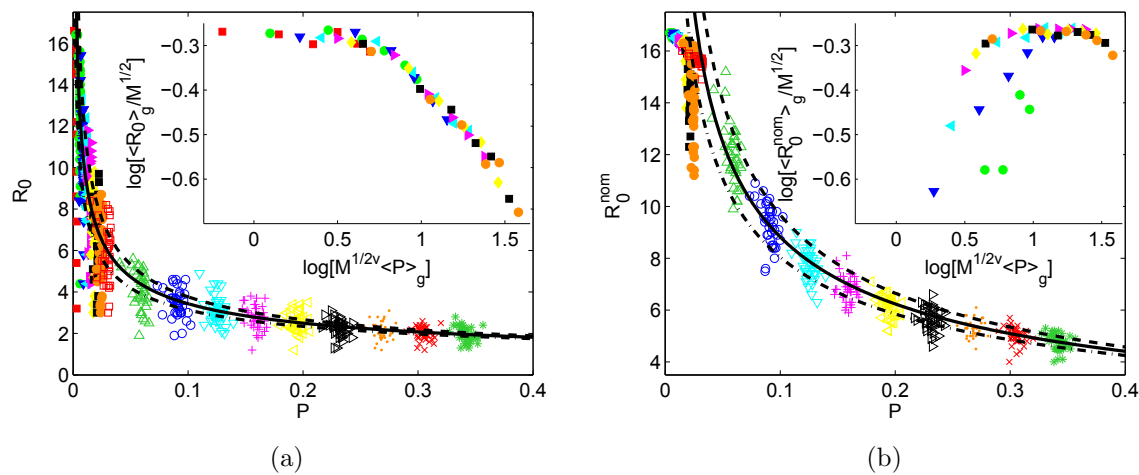


**Figure 5.** (a) The length scale  $R_0$  is plotted versus  $P$ ; a power law fit is shown with a solid line, and dashed lines are used for  $\nu = 0.46 \pm 0.04$ . The inset shows the finite size scaling collapse for  $\nu = 0.46$ . (b) Same, but for the nominal length scale  $R_0^{\text{nom}}$  and  $\nu = 0.5 \pm 0.04$ , with the inset showing a collapse for  $\nu = 0.5$ . Symbol colors are consistent with those used in figure 4.

susceptible to system size effects. Furthermore, a length scale only truly diverges at a critical point in the infinite system limit, so establishing a length scale which becomes the system size in a finite system near the critical point begs the question, is this length finite at the critical point but just larger than any system size we have studied? The purpose of finite size scaling is to isolate the functional form of the length scale in the infinite system limit by scaling out the dependence on the system size. First assume a form

$$\langle R_0 \rangle_g = L \cdot g \left( L^{1/\nu} \langle P \rangle_g \right)$$

Here  $L = \sqrt{M}$  has been used as a measure of the system size. The scaling form should be the same for any system size, for an appropriate choice of the value of  $\nu$ . The above scaling has been studied for several values of  $\nu$  near the value given by the power law fit, including the mean-field value. The inset of figure 5 shows the finite size scaling collapse at low pressure. There is a noticeable difference in the quality of the collapse for different system sizes for  $\nu = 0.42, 0.46$  and  $0.50$  with the best collapse being for  $\nu = 0.46$ . Figure 6 shows the finite size collapse over the entire range of  $P$  for these exponents. For  $\nu = 0.42$ , the collapse fails in the mid-range of the tail, while for  $\nu = 0.50$  the collapse begins to fail in the knee of the scaling form as well as the tail. The collapse for  $\nu = 0.46$  seems to be the best compromise between the two. The deviation of the exponent from mean-field is significant but small, possibly reflecting logarithmic corrections, which we will explore further in section 8.

To better understand the deviation from mean-field, let's return to the bulk-surface argument discussed in 3. The  $R_0$  extracted from the numerics and used thus far in the discussion of the exponent  $\nu$  is found by identifying  $\delta n(R_0) = 0$ , where  $\delta n$  is the nullity

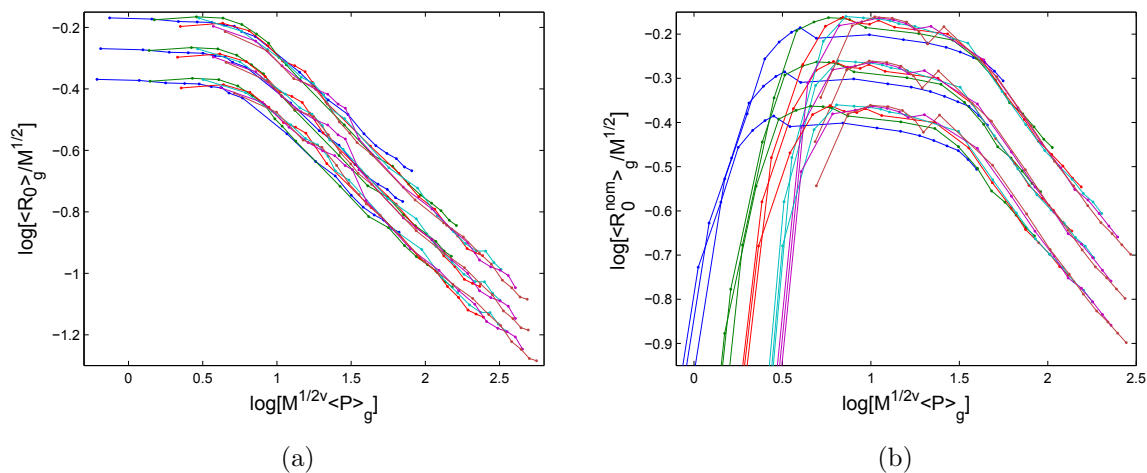


**Figure 6.** Presented in (a) is the finite size scaling collapse for  $\nu = 0.46 \pm 0.04$ . The lowest curve is for  $\nu - 0.04$ , the middle curve for  $\nu (= 0.46)$ , and the top curve is for  $\nu + 0.04$ . The curves are artificially offset vertically and horizontally. Figure (b) shows similar finite size scaling plots for  $R_0^{nom}$ , with  $\nu = 0.50 \pm 0.04$ .

of the linear system that describes the subregion of the packing of size  $R$  found from the SVD. Let's define a nominal nullity  $\delta n_{nom}$  which is simply  $n(R) - m(R)$ , where  $n(R)$  is the number of contacts inside a boundary of size  $R$  and  $m(R)$  is the number of grains inside and on the boundary, so that  $\delta n_{nom}$  is the expression for the mean field bulk-surface argument presented in Section 3. If the mean field approximation discussed in Section 3 is valid, the equality  $\delta n = \delta n_{nom}$  should hold. In fact,  $\delta n_{nom}$  does not equal  $\delta n$ , and what's more, a  $R_0^{nom}$  extracted from  $\delta n_{nom}$  reproduces the mean-field result. Figures 5 and 6 also show the results for  $R_0^{nom}$ . Since so much of the data at low pressures saturate at the system size for  $R_0^{nom}$ , it is difficult to do a power law fit as with  $R_0$ , even for the largest system size. The power laws plotted for  $R_0^{nom}$  are not taken from a fit. Instead, the exponent 0.5 is verified using finite size scaling only. For small  $M^{1/2\nu} \langle P \rangle_g$  none of the collapses do well. If one focuses only on the plateau and tail, the collapse for  $\nu = 0.46$  fails particularly in the plateau and near the knee, while  $\nu = 0.54$  fails in the tail.  $\nu = 0.5$  seems to be the best balance between the two. The finite size scaling for  $R_0$  works well over a larger range, including the plateau.

As an additional test of the the finite size scaling collapse used to verify the exponent  $\nu$ , one can also focus on the tail of the collapse. In the tail, one expects  $\langle R_0 \rangle_g / M^{1/2}$  to exhibit a power law dependence on  $M^{1/2\nu} \langle P \rangle_g$ . If the exponent of this power law and the exponent used in the finite size scaling differ, this leads to a failure of the collapse at different system sizes. However, within the limits set by the variance in the data due to the sensitivity of the collapse on the exponent used, the tail of  $\langle R_0 \rangle_g / M^{1/2}$  should have a slope corresponding to the infinite system size exponent. This can be seen by assuming a power-law form for the scaling function, and using  $\nu_t$  as the “test” exponent

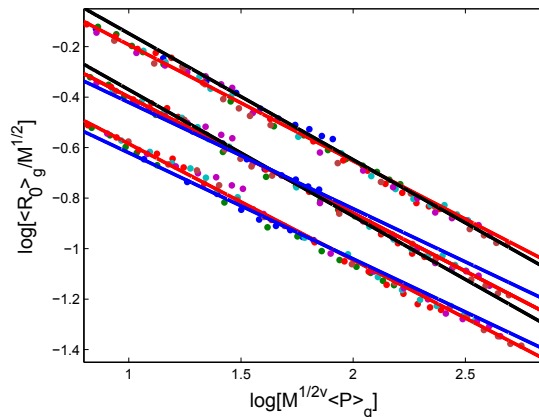


**Figure 7.** As with figure 6, the finite size scaling collapse is shown. The lines connecting data points at the same system size are no longer shown, but symbols use the same colors, and the same vertical shift is used. Blue, red, and black lines have slopes 0.42, 0.46, and 0.50 respectively.

used to collapse the finite system size data:

$$\langle R_0 \rangle_g = M^{\frac{1-\nu/\nu_t}{2}} \langle P \rangle_g^{-\nu}$$

Because  $\nu_t$  is only applied to the system size variable  $M$ , the pressure depends on  $\langle R_0 \rangle_g$  only through  $\nu$ . Figure 7 shows the finite size collapse for the test exponent equal to 0.42, 0.46, and 0.50. In all three cases, a line with a slope of 0.46 seems to agree best with the data, suggesting that  $\nu = 0.46$  is in indeed the exponent in the infinite system size limit.

The recovery of the mean-field exponent for  $R_0^{nom}$  implies something very interesting about the bulk-surface argument. The mean-field result for  $\delta n_{nom}$  as presented in Section 3 has a form  $\alpha P^{1/2} R^2 - \beta R$ . Even if the nullity from SVD,  $\delta n$ , differed from  $\delta n_{nom}$  by a term linear in  $R$ , the functional form of the length scale wouldn't change. The difference in exponents for  $R_0$  and  $R_0^{nom}$  must be the result of a novel  $P$  dependent term in the bulk-surface argument for  $\delta n$ :  $\delta n - \delta n_{nom} = P^{-1/2} f(P^{1/2})$  for some unknown function  $f$ . Figure 8 suggests that scaling forms for both  $P^{1/2} \delta n$  and  $P^{1/2} \delta n_{nom}$  exist and are functions of  $\langle R \rangle_g \langle P^{1/2} \rangle_g$  only. But, the scaling form of  $\delta n_{nom}$  is a quadratic over the entire data range, even below the cusp at  $\langle R_0^{nom} \rangle_g \langle P^{1/2} \rangle_g$ , while  $\delta n$  fails to be quadratic near  $\langle R_0 \rangle_g \langle P^{1/2} \rangle_g$ . Section 8 discusses four distinct sources of disagreement between  $\delta n$  and  $\delta n_{nom}$ .

## 7. Modelling the PTS

### *Geometry of the FNE Solution Space*

The set of solutions to Eq.5 sampled by the random walk make up a high dimensional vector space. Two separate but related spaces are discussed here. The more commonly



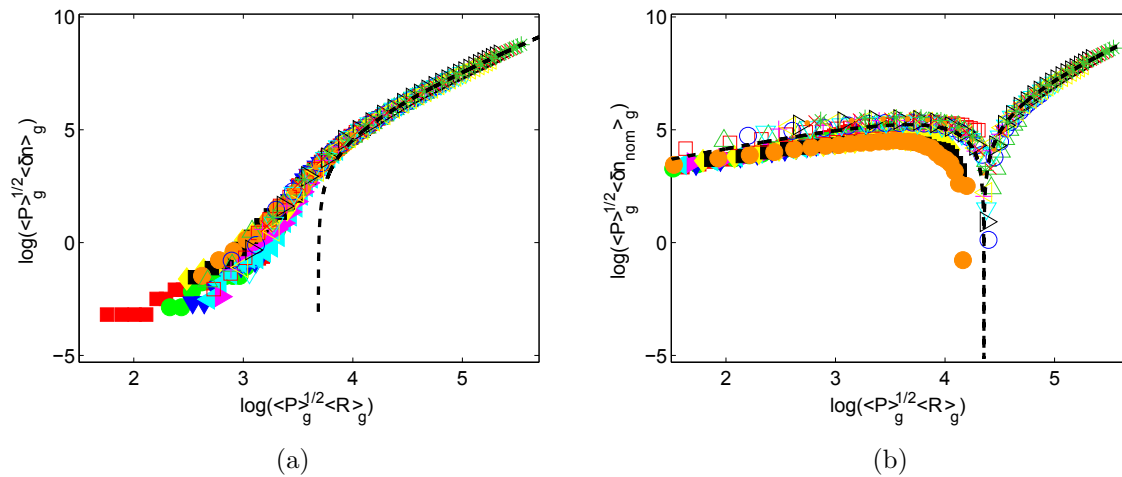


**Figure 8.** (a) Collapse of  $\delta n(R)$  after scaling with  $P$ . The quadratic fit (dashed line) is not shown over the entire data range because for low  $P^{1/2}R_0$  the fit becomes negative, while  $\delta n(R)$  is always positive. (b) Same scaling for  $R_0^{nom}$ . A quadratic fit agrees with the data well over the entire data range. Symbol colors are consistent with those used in figure 4. As before, open symbols range from 0.01 to 0.1 and filled symbols from 0.001 to 0.008.

discussed space is the “force space,” a  $z$  dimensional space where each axis corresponds to a different contact force magnitude[13]. Not every point in this space is a solution. However, there are bounds on where solutions can be located in the force space. The positivity constraint confines all solutions to the  $\{f_1 \dots f_z\} \geq 0$  hyper-octant. Additionally, a linear global constraint, say from fixing the pressure, is generally applied to the FNE, so that there is at least one constraint of the form  $\sum_{i=1}^z c_i f_i = C$ , where the  $c_i$ 's and  $C$  are some constants from the geometry of the packing, for instance the center-to-center separations of the disks for the pressure constraint. Ignoring the ME constraints for a moment, the linear global constraints require that at least one  $f_i$  be non-zero. In principle, there can be solutions where  $f_i = C$  while  $f_{j \neq i} = 0$ . This provides the point of intercept with each axis of the force space. Since the global constraints are linear, each intercept is connected by a line, forming a high dimensional polytope (polytope).

Contained within this polytope are all of the valid force networks for the given MS, although much of the space within this polytope does not correspond to valid solutions. The vertices, for instance, which are the intercepts with the  $f_i$  axes, cannot be solutions. They correspond to force networks where  $f_i = C > 0$  and  $f_{j \neq i} = 0$ , which is never a force network that satisfies ME.

It is possible though to apply the ME constraints by further changing the shape and dimensionality of the polytope. Beginning with the polytope defined by only the global constraint and some valid force network, choose a ME constraint which is applied to grain  $i$  with  $z_i$  contacts. Such a constraint relates  $z_i$  contact forces linearly, so it is represented geometrically as a  $z_i$  dimensional (unbounded) polytope. Each ME constraint allows

$f_i = 0$  as a solution, so the ME polytopes intersect the origin. Therefore, an ME polytope is never entirely embedded in the global constraint polytope. Once imbedded in the force space, the intersection of *all* such ME constraint polytopes with each other as well as the global constraint polytope represents the set of valid force networks. The polytope that results from these intersections contains what will be referred to as the “solution space,” equal in dimension to the nullity of  $A$ . The solution space is simply connected because of the linearity of the forces: the sum of any two force networks is also a valid force network, and properly normalized will satisfy the global constraint. The solution space is also likely convex; [13] claims that the force space is “trivially” convex, also due to the linearity, but fails to take into account the positivity constraint when coming to this conclusion. The positivity constraints have similar implications for the solution space: while linear superpositions of valid force networks do result in valid force networks, they do not necessarily result in contact forces which are all positive. However, an assumption of convexity allows us to estimate the number of valid force networks at a given pressure, as which we now explain in more detail.

Particular properties of the solution space are dependent on the MS. But, a useful approximation is that the solution space is enclosed by a hypersphere of dimension  $\delta n$ . Since, in FNE, each valid force network is considered to be equally likely, and the solution space is simply connected, the volume of the  $\delta n$ -dimensional hypersphere estimates the number of solutions. The radius of the hypersphere for solutions within a bounded region of linear size  $R$  is  $\langle \eta(R) \rangle$ , the average distance from  $\vec{f}_0(R)$  to a point on the hypersphere. When  $\delta n > 2$ , a random walk through the solution space beginning at  $\vec{f}_0(R)$  is transient; that is to say, the walker will rapidly approach the surface of the hypersphere, and spend the majority of its time there. This reflects the geometric property of high dimensional polytopes which is that the majority of its volume is concentrated near the boundary. As the dimension  $\delta n$  becomes larger, a good approximation of  $\langle \eta(R) \rangle$  results from sampling  $\vec{f}(R) - \vec{f}_0(R)$  over the random walk steps:  $\langle \eta(R) \rangle = \left\langle \left| \vec{f}(R) - \vec{f}_0(R) \right| \right\rangle$ . This is essentially a radius of gyration for the high-dimensional random walk, and a similar quantity has been used previously as a measure of force indeterminacy[15].

The volume of the hypersphere plays an essential role in the understanding of the unjamming transition as a critical point. As  $R \rightarrow R_0$ , the hypersphere shrinks, both in linear size  $\langle \eta(R) \rangle$  and in dimension, to a single point that is the only solution to the precisely determined linear system of ME equations. Since, as shown earlier,  $R_0$  becomes the system size as  $P \rightarrow 0$ , if the volume of the hypersphere is a measure of the number of valid force networks available, then the entropy of valid force networks goes to zero as  $P \rightarrow 0$ . The unjamming transition is associated with a point at which there are no solutions available to Eq.5.

*Some Results Based on the Solution Space*

In this section we'll discuss a model of  $\eta(R)$  and  $C(R)$  based on properties of the solution space. These results will be based on two approximations, concerning the typical values for the “magnitudes” of the force networks:

$$\left| \vec{f}_0(R) \right| = \left( \sum_{i=1}^{n(R)} f_{0,i}^2 \right)^{1/2} \approx n(R)^{1/2} [f_0] = \left| \vec{f}(R) \right| \quad (6)$$

and using  $\vec{f}(R) = \vec{f}_0(R) + \sum_{i=1}^{\delta n(R)} c_i \hat{g}_i$

$$\eta(R) = \left| \vec{f}(R) - \vec{f}_0(R) \right| = \left| \sum_{i=1}^{\delta n(R)} c_i \hat{g}_i \right| = \left( \sum_{i=1}^{\delta n(R)} c_i^2 \right)^{1/2} \approx \sqrt{\delta n(R)} [f] \quad (7)$$

The  $f_i$ 's are individual contact forces in the initial force network  $\vec{f}_0$ . The brackets  $[\ ]$  represent an average over elements of force networks (or geometry). For instance,  $[f]$  is the average contact force, and  $[z]$  is the average contact number for a particular MS. There are several assumptions used here. First, the contact forces themselves are uncorrelated; the sum over  $n(R)$  contact forces is simply  $n(R)$  times the average contact force. This assumption is particularly good for large force networks, and is based on the observation that contact forces do not seem to exhibit correlations beyond the size of a grain, where of course ME constraints limit what values they can take ([33] provides some arguments that support this observation. It is shown that the assumption of a uniform sampling of states leads to the decorrelation of contact forces at the isostatic point). The second assumption that is made is that all force networks at a given  $P$  have the same magnitude:  $\left| \vec{f}_0(R) \right| = \left| \vec{f}(R) \right|$ . This assumption is based on the fact that the pressure is fixed, so that the sum of the contact forces is fixed. Of course this is not equivalent to saying that the magnitudes (sum of squares of the contact forces) cannot fluctuate, but those fluctuations should still be controlled by  $P$ . Finally, the assumption is made that the coefficients  $c_i$  of the expansion of  $\vec{f}(R) - \vec{f}_0(R)$  in terms of the null space basis vectors are also uncorrelated and on average are equal to the average contact force, since  $[f]$  is the only force scale in the system.

The correlation function  $C(R)$  is related to  $\eta(R)$ , which can be seen by expanding  $\eta(R)^2 = \left| \vec{f}(R) - \vec{f}_0(R) \right|^2$ :

$$\left| \vec{f}(R) - \vec{f}_0(R) \right|^2 = f(R)^2 + f_0^2(R) - 2\vec{f}(R) \cdot \vec{f}_0(R) \quad (8)$$

so that

$$C(R) \approx 1 - \frac{\eta(R)^2}{2f(R)^2} \quad (9)$$

Using the results Equations 6 and 7, the correlation function  $C(R)$  is

$$C(R) \approx \frac{1}{2} \left( 1 + \frac{m(R)}{n(R)} \right) \quad (10)$$

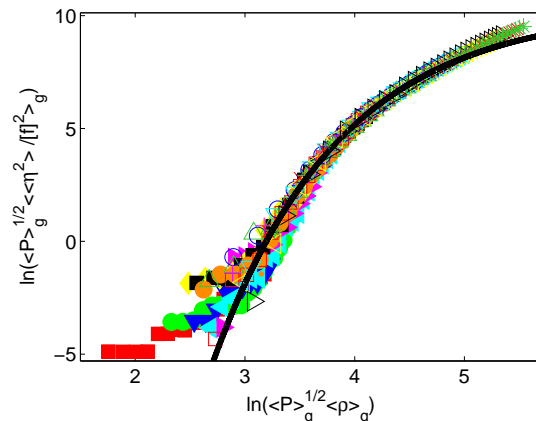


**Figure 9.** The collapse of  $\bar{\eta}^2(R)$  with pressure is shown. The solid line is a fit to  $G(y) = G_0 e^{-(b/y)^\alpha}$ , with  $b = 161$ ,  $\alpha = 0.86$ , and  $G_0 = 3 \times 10^4$ . Notice the similarity of this collapse to figure 8a, which illustrates the equality of  $\bar{\eta}$  and  $\delta n$  (equation 7). Symbol colors are consistent with those used in figure 4.

This is a valuable result because it suggests that the correlation function can be evaluated by simple counting:  $m(R)$  is the number of independent equations, and  $n(R)$  the number of independent degrees of freedom, of  $A(R) \vec{f}(R) = \vec{b}(R)$ . In the mean-field approximations of section 3,  $m(R)$  should be (twice) the number of grains in the subregion of size  $R$ , and  $n(R)$  should be the number of contact forces.

The approximate form of the correlation function also explains a peculiar property of the measurements of  $\langle\langle C(R) \rangle\rangle_g$  from section 6: the correlation function does not decay to zero. In the  $R \rightarrow \infty$  limit, and in mean-field,  $C(R) = \frac{1}{2} \left(1 + \frac{2M}{z}\right)$ , which is 1 at the isostatic point but is never less than 1/2. This is essentially the result of the positivity constraint. If contact forces could be negative,  $[f]$  would be zero when contact forces were uncorrelated. The average must always be greater than zero for compressive forces. Comparison of Eq. 10 with numerical results are presented in section 9.

## 8. Corrections to $l^*$

### *Logarithmic Corrections*

The deviation from the mean-field exponent of  $\nu = 0.5$  suggests that mean-field bulk-surface argument breaks down. In this section analysis of the behavior of  $\eta(R)$  is used to identify a logarithmic correction to the mean-field prediction. The radius of gyration normalized by the force scale,  $\bar{\eta}^2(R) = \eta^2(R) / [f]^2$ , collapses for different values of  $P$  according to the scaling form  $\langle P \rangle_g^{1/2} \langle \bar{\eta}^2(R) \rangle_g = G \left( \langle R \rangle_g \langle P \rangle_g^{1/2} \right)$  (see figure 9).

The hypersphere that encloses the valid force networks has a dimensionality  $\delta n(R)$ , which has been shown (Eq.7) to depend on  $\bar{\eta}(R)$ . Furthermore, the linear size of the hypersphere is  $\eta(R)$ . In order for the volume of the hypersphere to be a count of solutions to  $A(R) \vec{f}(R) = \vec{b}(R)$ , the linear size must be unitless, and so the unitless

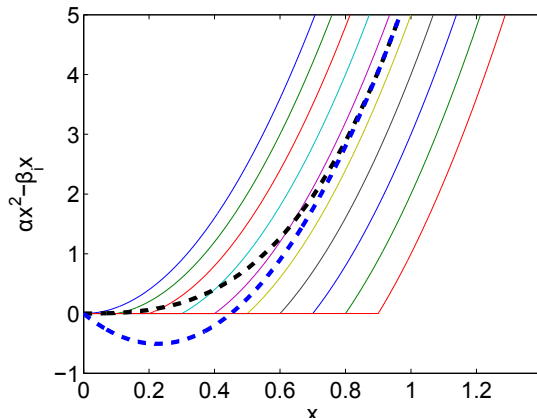


**Figure 10.** Ten truncated quadratic functions are shown. Below the root  $\alpha/\beta_i$ , each quadratic function is set to zero. The average of the functions is shown with a black dashed line, while the average of the untruncated quadratics is shown with a blue dashed line. The horizontal intercept of the black curve is at  $x = 0$ , but at large  $x$  the black curve has a quadratic form.

volume  $V(\langle\bar{\eta}\rangle_g)$  depends only on the average *normalized* radius of gyration. The number of solutions  $V(\langle\bar{\eta}\rangle_g)$  approaches 1 as  $\langle\eta\rangle$  decreases; the hypersphere shrinks in size and in dimension. But, there is always a single solution to ME, even at the isostatic point (where the linear system is precisely determined). Therefore, the entropy  $\ln(V(\langle\bar{\eta}\rangle_g))$  goes to zero when  $\langle\bar{\eta}\rangle_g$  goes to some small value  $\bar{\eta}_0$ .

It should be mentioned that  $\bar{\eta}_0$  only has an interpretation as an MS-averaged value. For any particular MS,  $\bar{\eta}$  is always zero when  $R < R_0$ . But, over many geometries at a particular  $\langle P \rangle_g$ , the value of  $R_0$  can fluctuate, and so  $\langle\bar{\eta}\rangle_g$  is only zero when  $R = 0$ . On the other hand, the volume of the hypersphere  $V(\langle\bar{\eta}\rangle_g)$  becomes 1 at a value of  $\langle R \rangle_g$  larger than zero since it is a function of  $\langle\bar{\eta}\rangle_g$  and not  $\bar{\eta}$ . This value of  $\langle R \rangle_g$  corresponds to a value of  $\langle\bar{\eta}\rangle_g$  which is greater than zero, but which controls the entropy-vanishing behavior of the solution space, and it is this value of  $\langle\bar{\eta}\rangle_g$  that is being referred to as  $\bar{\eta}_0$  (see figure 10).

Next we look more closely at the scaling function  $G(\langle R \rangle_g \langle P \rangle_g^{1/2})$ . For small values of  $y = \langle R \rangle_g \langle P \rangle_g^{1/2}$ , the scaling function is fitted well by  $G(y) = G_0 e^{-(b/y)^\alpha}$ , for fitting parameters  $\alpha$ ,  $G_0$ , and  $b$  (see caption for figure 9). At  $\langle\bar{\eta}\rangle_g = \bar{\eta}_0$ , the form of the scaling function implies

$$\langle P \rangle_g^{1/2} \bar{\eta}_0^2 = G_0 \exp \left\{ - \left( \frac{b}{\langle R_0 \rangle_g \langle P \rangle_g^{1/2}} \right)^\alpha \right\} \quad (11)$$

and solving for the length scale  $\langle R_0 \rangle_g$ ,

$$\langle R_0 \rangle_g^{-1} = \frac{\langle P \rangle_g^{1/2}}{b} \left( \ln \left\{ \frac{G_0}{\bar{\eta}_0^2} \right\} - \frac{\ln \left\{ \langle P \rangle_g \right\}}{2} \right)^{1/\alpha} \quad (12)$$

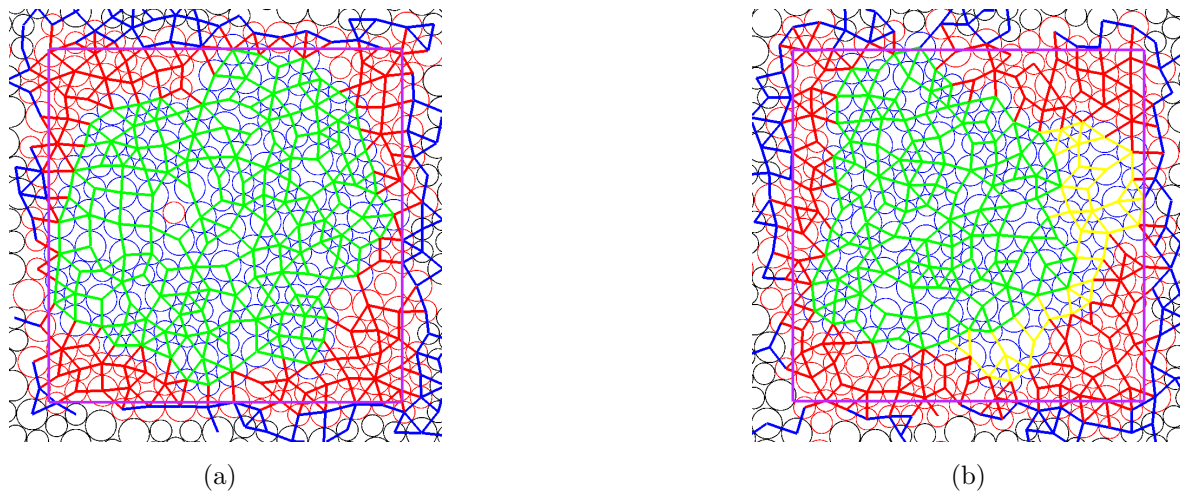


**Figure 11.** Figure a.) shows a 300 grain packing at  $\delta\phi = 0.01$ . Locally determined regions appear propagating inward from the boundary in red. b.) The same packing at  $\delta\phi = 0.006$  shows the onset of an isostatic cluster in yellow.

When  $\langle P \rangle_g$  is large, which in this case means relative to  $G_0$ ,  $\langle R_0 \rangle_g \propto \langle P \rangle_g^{-1/2}$ , recovering the mean-field result. However, when  $\langle P \rangle_g$  is small, the length scale exhibits a logarithmic correction:

$$\langle R_0 \rangle_g \propto \langle P \rangle_g^{-1/2} \left( \ln \left\{ \langle P \rangle_g^{-1/2} \right\} \right)^{-1/\alpha} \quad (13)$$

This result is based on the observation that for small  $y$ , the scaling function has an exponential form. This itself is at odds with the mean-field prediction. The product  $\langle P \rangle_g^{1/2} \langle \bar{\eta}^2(R) \rangle_g$  should be proportional to  $\delta n(R)$ , which mean-field predicts should be a quadratic function of  $R$ , and so  $G(y)$  should be quadratic in  $y$  as well. For large  $y$ , the scaling function is quadratic in  $y$  and so the mean-field prediction  $\langle R_0 \rangle_g \propto \langle P \rangle_g^{-1/2}$  is recovered. For small  $y$  on the other hand, the numerical results show that the mean-field bulk-surface argument breaks down and  $G(y)$  takes on an exponential form. For very small  $y$ , the quality of the collapse breaks down and correspondingly the fit becomes less convincing, but the deviation from the quadratic form has already emerged (compare to figure 8a).

The following sections explore some microscopic origins for the failure of the bulk-surface argument by analyzing the statistics of some microscopic properties of the MS configurations, as well as some sample packing geometries and the null spaces of their corresponding linear systems.

### *Local corrections to the Bulk-Surface Argument*

The first correction to the mean-field bulk-surface argument results from the vectorial nature of the ME equations. Unlike most constraint satisfaction problems, where each vertex or node contributes a single constraint on the variables which correspond to links associated with that vertex, with ME multiple equations describe force balance, further

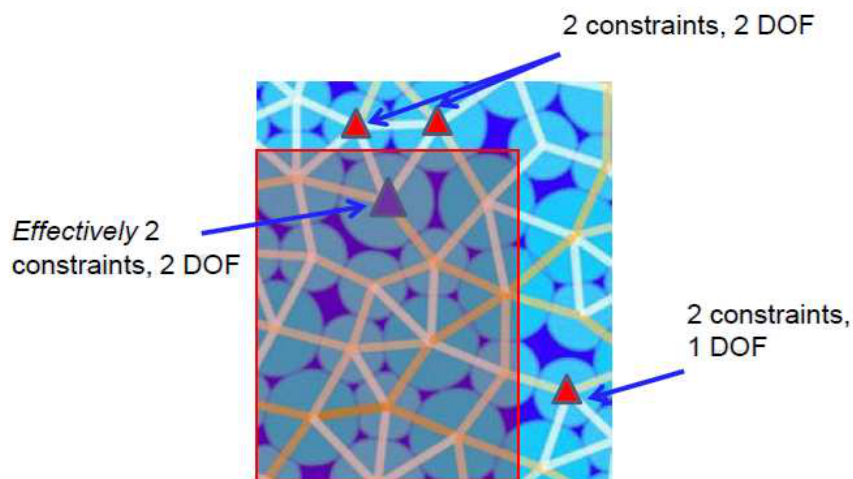


**Figure 12.** The red box in this example represents the boundary. While each grain corresponds to two ME constraints, sometimes a grain corresponds to less than three variable contact forces, such as the grains labelled with red triangles. The grain with a purple triangle has 2 constraints and *effectively* only two variable contact forces even though it has four contacts which lie inside the boundary. This is because two of the contact forces are already determined by the additional constraints from the boundary grains.

coupling the force degrees of freedom. Specifically, in 2D, there are two force balance equations associated with each grain. If a grain has only one force exerted on it, that force variable is *overdetermined*. One equation is all that is necessary to solve for the force variable, and the other equation is not necessary. This single force variable is known and is effectively not a variable at all. In 2D, the same happens when a grain has two force variables. The two equations of ME can be used to define both force variables. Only grains with three or more contacts are undetermined. In a packing without a fixed boundary, there are never grains with less than three contacts. However, when there is a boundary defined by a set of additional boundary constraints, grains with only one or two force variables are possible (see figure 12).

At low pressure the effect of the boundary grains which involve one or two force variables also tend to completely define the contact forces of neighboring grains. This allows for the phenomenon of effectively defining force variables near the boundary to propagate into the interior of the subregion, and at lower pressures this effect propagates further into the interior (see figure 11). A recursive algorithm is used to find these effectively determined force variables. All of the grains with two or less force variables are found, and then all remaining grains, with two or less forces after taking into account these effectively determined forces, are found. This process is repeated until all effectively determined force variables are found.

These effectively determined forces and corresponding ME equations both contribute corrections to the bulk-surface argument. The dependence of these corrections is roughly linear as a function of  $R$ , but the slope has a dependence on

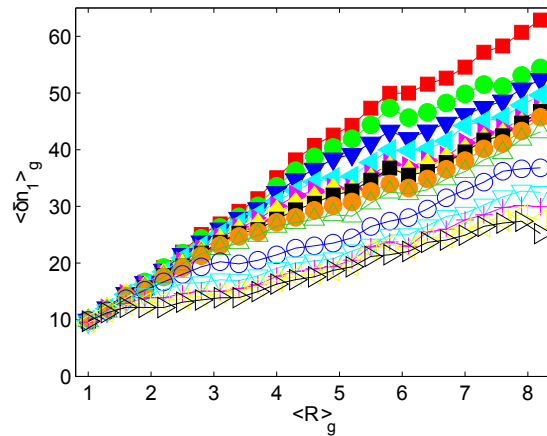


**Figure 13.** The local correction,  $\delta n_1$ , is the difference between the number of ME equations and the number of determined force variables (the red regions of the packings). The curves are not quite linear, and depend on  $P$  in a non-trivial way. There doesn't appear to be a single scaling, although different ranges of data can be scaled with  $P$ . Symbol colors are consistent with those used in figure 4.

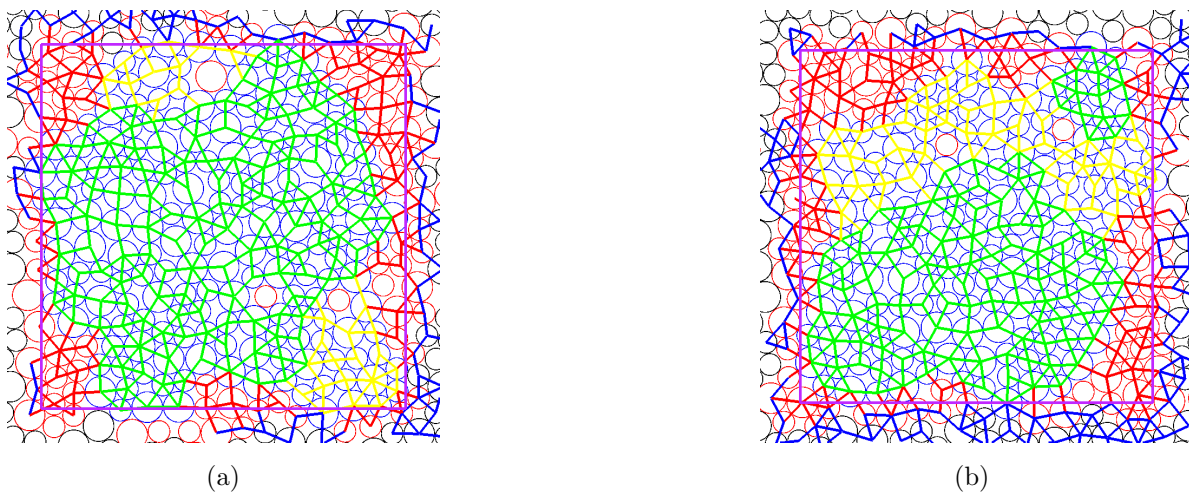


**Figure 14.** a.) Isostatic clusters are not always connected. Here there are two separate isostatic clusters. b.) On the other hand, underdetermined clusters, the green regions, are not always connected either. For each independent green cluster, there is an additional set of constraints from the stress tensor.

$P$  (figure 13).

### *Cooperative corrections*

While the local corrections to the bulk-surface argument are the most important contributions to the bulk-surface argument, they are not the only corrections. A second important correction comes from isostatic clusters of grains which are embedded inside the boundary of size  $R$ . Generally, there are sometimes one (or more) connected sets of grains within the boundary whose ME equations together define a linear system which



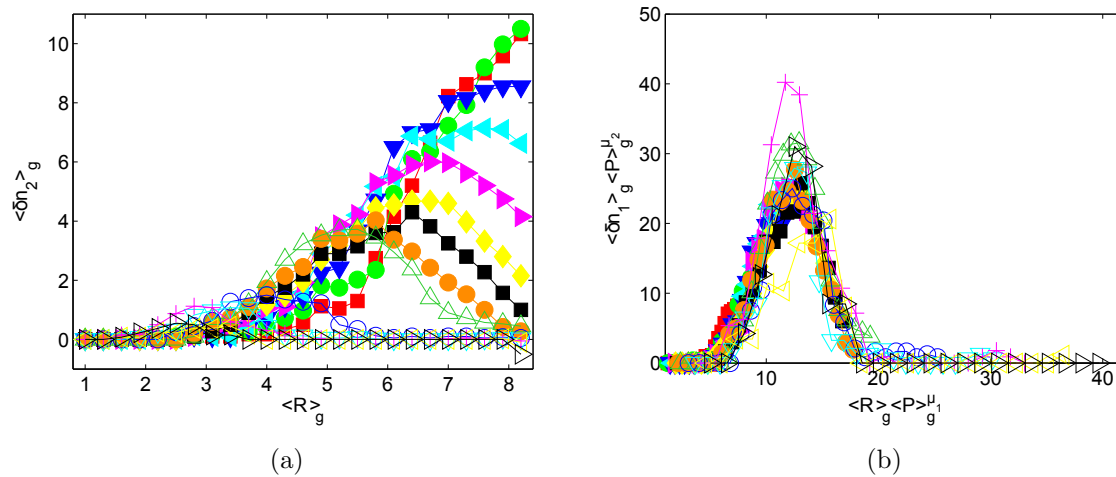


**Figure 15.** In figure a.) the isostatic cluster correction  $\delta n_2$ , which is the difference between the number of ME equations and the number of determined contacts, associated with one of the isostatic (yellow) clusters. b.) a scaling does exist to collapse this data well;  $\mu_1 = 0.4$  and  $\mu_2 = 1$ . Symbol colors are consistent with those used in figure 4.

completely determines the corresponding set of force variables. This set of grains is not necessarily the entire set of grains within the subregion (if it was, the nullity would be zero). In addition, linear subsystems embedded within these isostatic clusters are typically underdetermined, meaning that the linear subsystems defined by these clusters cannot be reduced to local effects like those due to the corrections discussed previously.

In addition to having a  $P$  dependence, these cluster contributions to the bulk-surface argument are not linear in  $R$ , but do exhibit scaling with the pressure (figure 15).

### *Multiple independent clusters*

The combination of locally determined force variables and isostatic clusters occasionally leads to a fracturing of the subregion defined by  $R$  into multiple underdetermined clusters (i.e., clusters of force variables which can be changed while satisfying ME). A third, and less important, correction results from the number of distinct underdetermined clusters. To be clear, these clusters are *not* the yellow isostatic clusters. For each cluster of underdetermined forces, the set of determined boundary forces defines a local stress tensor. Because this stress tensor is fixed as long as the boundary forces cannot change, the three components (in 2D) of the stress tensor provide additional relationships between the otherwise independent equations of ME which make up the linear system associated with the underdetermined cluster, reducing the total number of independent equations by three. These fractured subregions do not occur frequently enough to be characterized statistically in a quantitative way, but they clearly become more common as the pressure is lowered.

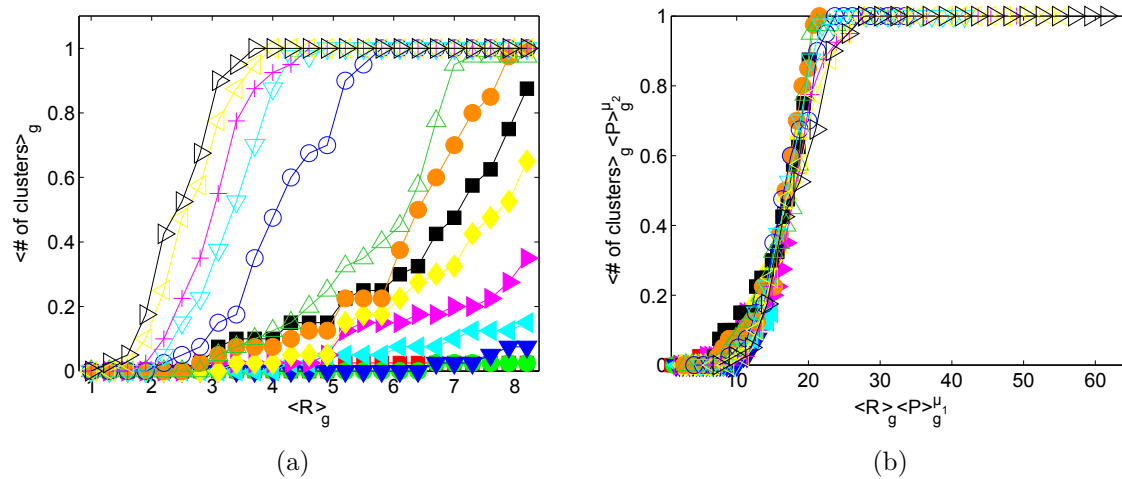


**Figure 16.** The number of clusters rarely becomes greater than 1 for this system size, and so the 2-cluster packings are averaged out during geometry-averaging. Figure a.) shows the number of clusters, while figure b.) shows a simple scaling of the horizontal axis with  $\mu_1 = 0.5$  and  $\mu_2 = 0$ . This is to be expected, since the number of clusters goes from 0 to 1 as soon as  $\delta n$  becomes non-zero. The scaling of the horizontal axis reflects the scaling with  $R_0$ . Symbol colors are consistent with those used in figure 4.

A simple algorithm is employed to count the number of independent clusters. First, the algorithm chooses a grain which is undetermined (meaning a grain whose ME equations are not involved in either a locally determined or an isostatic cluster). Then, it builds a set of grains out of this first grain’s neighbors, and repeats this process with the new grains until the set includes the neighbors of each other grain in the set or a boundary grain, which has all determined forces. Then the algorithm restarts with a grain not included in the previous set. It continues to build these new sets until all of the undetermined grains have been exhausted. The number of times the algorithm restarts is the number of independent clusters.

### *Locally crystalline*

Finally, even after the previously discussed corrections to be bulk-surface argument are taken into account, there are very rarely special cases where a single force variable shared by two grains can be determined (in the sense that it is already known), even though none of the other force variables associated with those grains are. This may seem counter intuitive. All of the previously discussed phenomena involve a boundary effect where a grain whose force variables are all determined is in contact with a grain whose force variables are not all determined. At first, it might seem that if all of a grain’s contact force variables can change but one, there is no reason why that one should not fluctuate as well. In the special case of crystalline order, though, we know from experience with the “wheel move” that the ME equations are not all independent, leading to additional “breathing” modes. Take, for instance, the localized wheel move

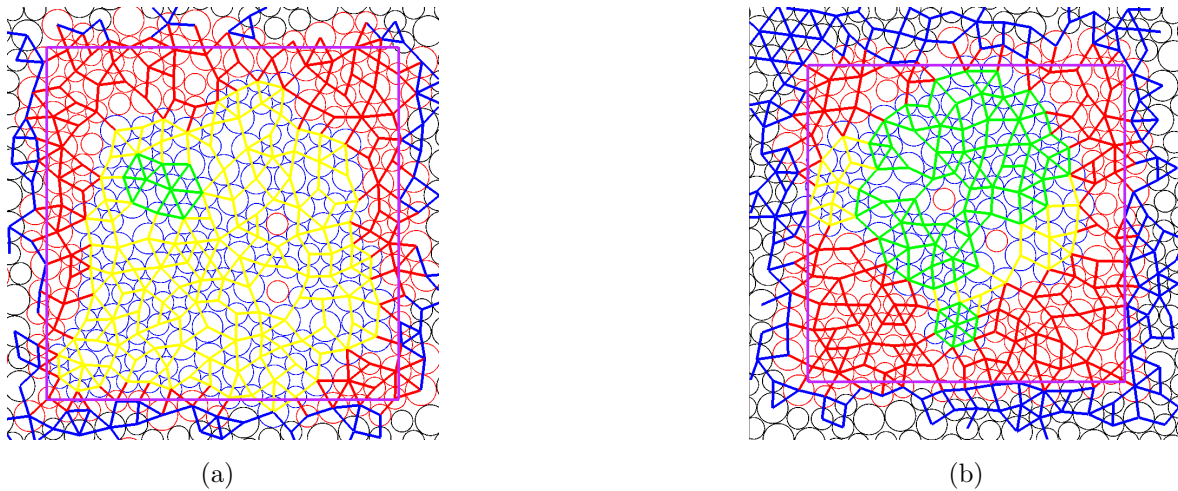


**Figure 17.** Figure a.) shows an extremely localized underdetermined cluster (green). The isostatic cluster has propagated far into the bulk of the packing, leaving only a small cluster to fluctuate. In the bottom of figure b.), there is a crystalline cluster, separated from the main cluster by two isolated yellow bonds. At first, it may seem odd that those yellow bonds are considered determined. It turns out, though, that these yellow bonds, along with the crystalline cluster, form an isostatic cluster. Because of its symmetry, however, the crystalline cluster can still fluctuate according to wheel moves. For this packing, the null vectors have been analyzed, and the crystalline cluster is in fact a wheel move and no other types of fluctuations are allowed.

type cluster in the bottom of figure 17. There are 14 ME equations associated with this cluster, and including the two yellow links which point upward (and are shared between grains which also contain undetermined force variables, which is what makes this example unique) there are 14 force variables. Assuming the two vertical links do indeed correspond to determined variables, the wheel move still allows for the 12 internal green links to fluctuate without changing any of the other forces, simply because of the added symmetry of the triangular lattice. Or, to put it another way, because the ME equations associated with a crystalline structure are not all independent, some forces must be determined and the SVD essentially “chooses” to localize the basis on the crystalline structure and never allow the boundary force variables to fluctuate. Because the wheel move is in some sense a different underdetermined cluster, it does count towards the total number of underdetermined clusters. But, since it is not separated from the main cluster by determined grains, only some particularly fortuitous determined forces, it is not detected by the cluster detection discussed in 8.

It is not enough to simply have crystalline structure; the crystalline structure must be surrounded by fixed forces as well, or there would not be an independent set of stress tensor constraints on the cluster and so would be indistinguishable from the main cluster. As a result, these wheel move clusters appear to be extremely rare; too uncommon, in fact, to allow for meaningful statistics.

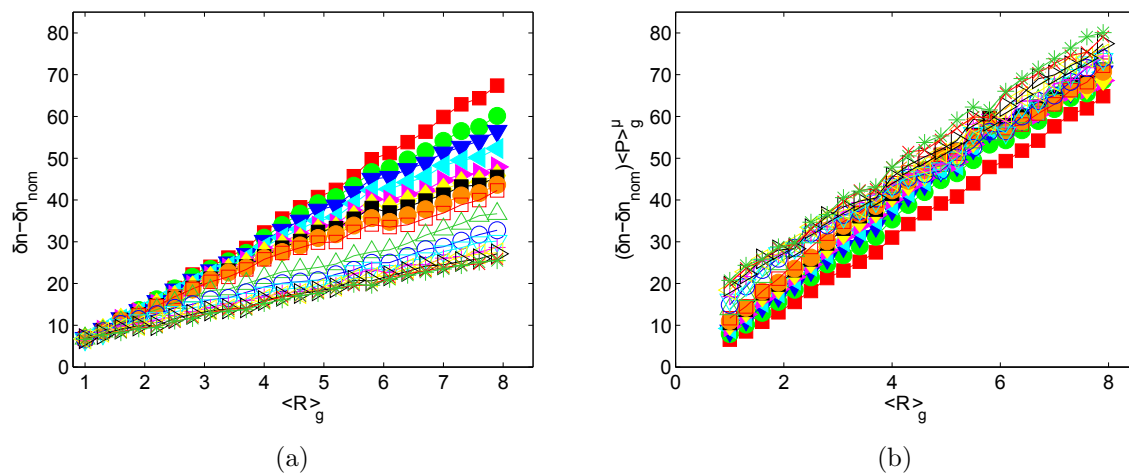


**Figure 18.** a.) The total correction to the nominal nullity is shown, which is linear in  $R$  but has a  $P$  dependence. b.) The correction scales with  $P$ , with an exponent of  $\mu = 0.25$ . Symbol colors are consistent with those used in figure 4.

### Net Corrections

In figure 18 the difference between  $\delta n$  and  $\delta n_{nom}$  is shown. The difference  $\delta n - \delta n_{nom}$  represents the total correction to the bulk-surface argument, which takes the form  $\delta n_{nom} = aR^2P^{1/2} - bR$  for constant  $a$  and  $b$  (the effects of slight variations in packing fraction are being ignored). The correction  $\gamma(R, P) = \delta n - \delta n_{nom}$  amounts to an additional term in the bulk-surface argument:  $\delta n = aR^2P^{1/2} - bR + \gamma(R, P)$ . If this term were to be either linear and independent of pressure, or quadratic and dependent on the square root of pressure, the mean-field exponent  $\nu = 0.5$  would be recovered. As seen in figure 18, neither is the case.  $\gamma(R, P)$  is linear in  $R$ , with a slope of  $P^{-1/4}$ , and a pressure dependent vertical intercept  $Y(P)$ . The bulk-surface argument, then, has a form  $\delta n = aR^2P^{1/2} - (b - P^{-1/4})R + Y(P)$ , which does not have a root of  $R_0 \propto P^{-1/2}$ . Even though there is no theory predicting this form for  $\delta n$ , it's worth noting that RFOT would predict a free energy as a bulk-surface competition with a temperature dependent surface tension [9] (in analogy to the pressure dependent coefficient of the linear term found here).

This section is concluded with an illustration of the clusters that emerge in a single packing as the pressure is lowered (figure 19). The figure caption addresses the particular characteristics of each step in the decompression.

## 9. Discussion

This article has detailed a new measure of correlations that arise in jammed granular systems. The model system is the force network ensemble constructed on geometries of compressible frictionless disk packings. The correlation function that has been introduced probes the effects of boundaries on mechanically stable packings, and

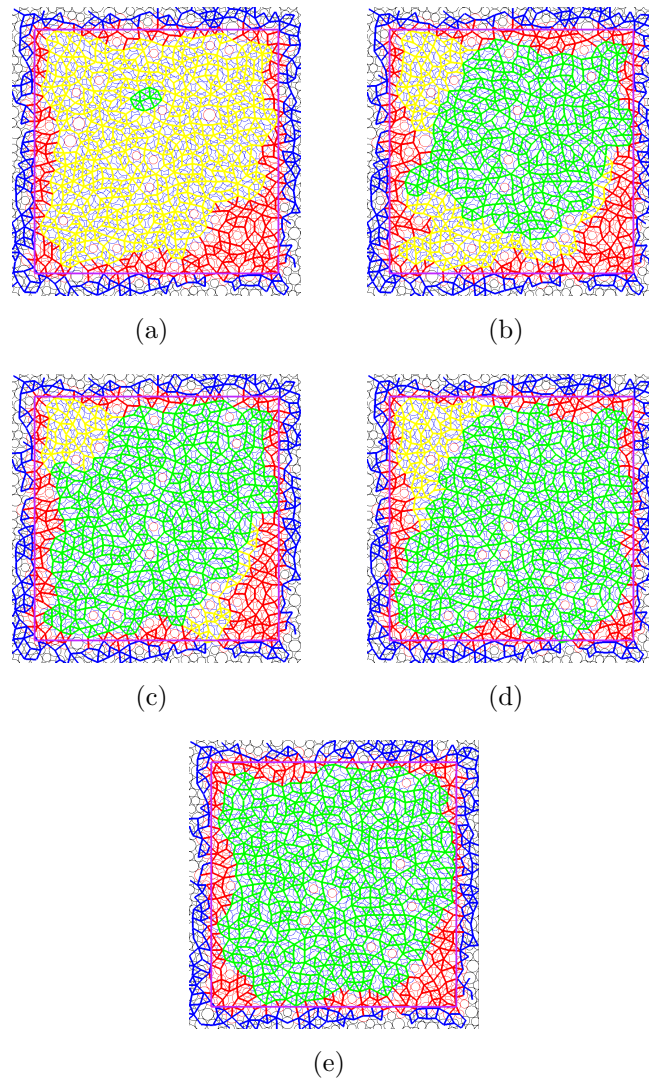


**Figure 19.** A single 900 grain trajectory is shown here.  $R$  is kept fixed as  $\delta\phi$  is increased. a.) the pressure is the lowest, and the isostatic cluster is nearly the size of the system. Also, the red regions propagate the furthest into the bulk. b.)  $\delta\phi$  has been doubled, from 0.001 to 0.002, and the isostatic cluster has fragmented into two clusters. c.) the isostatic clusters have shrunk considerably as the undetermined cluster grows. d.) One of the isostatic clusters has disappeared; on the other hand, the remaining cluster has grown somewhat. e.) at  $\delta\phi = 0.007$ , the isostatic clusters have disappeared entirely.

identifies a length scale that diverges as the packing unjams. A description of the unjamming transition as a critical point is developed based on the configurational entropy of equivalent mechanically stable force configurations.

The configurational entropy is itself based on a solution space picture where the mechanically stable force networks fill a configuration space that shrinks in size and dimension as the packings unjam. The length scale is shown to result from this entropy loss. A comparison of this length scale to the mean-field predictions of a popular bulk-surface argument has shown that the true exponent associated with the diverging length

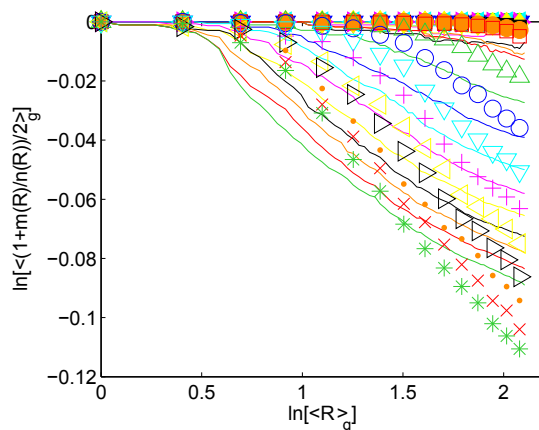


**Figure 20.** The results of Eq.10 are shown here, with numerical results for the corrected values of  $m(R)$  and  $n(R)$  used.  $\langle\langle C(R)\rangle\rangle_g$  is shown for reference. There is qualitative agreement with the model and  $\langle\langle C(R)\rangle\rangle_g$ , but with logarithmic scaling of the axes, the model does not seem to capture the power-law form of the tail. Symbol colors are consistent with those used in figure 4.

scale deviates from the mean-field prediction of 0.5. Analysis of the configuration space shows that this deviation is the result of the failure of the bulk-surface argument itself. Analysis of microscopic properties of the packings show that the failure of the bulk-surface argument is the result of additional terms which when taken together are linear in  $R$  but depend on pressure with a novel exponent. The bulk-surface argument relies on all ME constraints to be independent of each other, an assumption which is shown to fail in 2D disk packings close to the unjamming transition.

The correlation function  $C(R)$  is measured directly in numerics, and exhibits two regimes. The first is a plateau at  $C(R < R_0) = 1$ , and the crossover between this plateau and the tail of  $C(R)$  identifies the length scale. The tail  $C(R > R_0)$  is also described by a model based on properties of the solution space. Here we revisit Eq.10. One important result of section 8 is that a simple counting of all contacts and grains within the boundary of size  $R$  is not sufficient to characterize the number of free variables and constraints, since some constraints are not independent. Instead, an analysis of the null space of  $A(R)$  is used to identify the true number of free variables (the nullity) and algorithms are developed to find the independent constraints. It is these quantities which must be inserted into Eq.10, and so it is only at this point that Eq.10 can be compared to the direct measurements of  $\langle\langle C(R)\rangle\rangle_g$  (see figure 20). Eq.10 is in rough agreement with the measurements of  $\langle\langle C(R)\rangle\rangle_g$ , in that it captures exactly the same length scale (by construction), and decays similarly to  $\langle\langle C(R)\rangle\rangle_g$ . But, it fails to capture the power-law form of the tail, or agree quantitatively with the tail.

There is still a great deal of work left to do. For instance, while many microscopic sources of corrections to the mean-field bulk-surface argument have been identified, there is no proof that they have all been found. Are there other types of dependencies between constraints, for instance in much larger systems or much closer to the critical point, that

arise? What is the form of  $Y(P)$ , and how does it affect the exponent  $\nu$ ? Since the constraints become dependent, this suggests that there is some loss of randomness or disorder in the packings as the critical point is approached. One question that arises is whether or not an order parameter can be constructed based on these observations. In addition, the question of the importance of dimensionality is not addressed, since only 2D systems have been studied.

The mean-field corrections that are explored in section 8 identify structures within the packing that grow larger as the unjamming transition is approached. The immediate result of these observations is that the mean-field exponents do not apply. What's more, correlations lead to the emergence of precisely determined contact forces over larger scales when a packing is closer to unjamming. Is there, for instance, a renormalization group approach that could predict the observed exponent?

Also of interest is how grain shape affects the nature of the PTS correlations that arise in jammed packings. Specifically, we have considered 2D packings of elliptical grains, which are known to be *hypostatic*[34]. That is to say, elliptical grain packings, even when highly overcompressed, have less contacts than required for rigidity by the isocounting procedure when accounting for additional torque balance constraints. Nonetheless, elliptical grain packings are found to be mechanically stable. One possibility is that elliptical grain packings are ordered in a non-obvious way that leads to linear dependencies between ME equations (including torque balance equations). Through direct numerical analysis we have verified that such packings are in fact "critical": we always find exactly the same number of contacts as linearly independent constraints in ellipse packings and so the PTS correlation length as described in this work is the size of the system. This result holds in every case that we've checked below  $[z] = 6$ , which is the prediction from the isocounting procedure. At overcompressions resulting in  $[z] > 6$ , elliptical grain packings begin to exhibit underdetermined contact forces (see figure [?]). And so an intriguing question arises: do elliptical grain packings exhibit a line of true critical points from the marginally jammed, hypostatic packings up to  $[z] = 6$ ? Or, is there a more appropriate construction of the PTS correlation function that describes unjamming of elliptical grain packings?

Finally, a good deal of theoretical work concerning the solution space is left undone. Does a convincing argument exist that the solution space is convex, and if it is not, what are the implications for the approximation of the solution space as a roughly hyperspherical structure? There also may be instances where the solution space is not isotropic, for instance when packings are under shear, and the weights used in sampling of the solution space may very well be important. This work always applies a flat measure to the solution space, so that each force network is equally likely. In RFOT, it is acknowledged that the free energies of different glass states are not the same, and so some states are much more likely than others. In fact, the length scale derived from the PTS correlation function in RFOT relies on this distribution of free energies, and the length scale is extracted from the tail of the PTS correlation function rather than from the plateau. An interesting challenge for the granular PTS correlation function

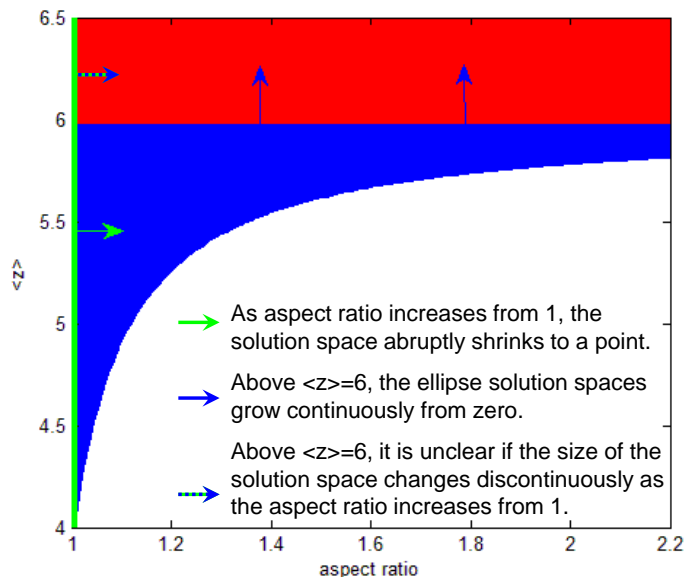


**Figure 21.** A schematic of an elliptical grain phase diagram exhibits several important regions. The region in white is unjammed, while the vertical green line represents disk packings (aspect ratio 1) which are jammed from  $z_0 = 4$ . In the blue region hypostatic ellipse packings are mechanically stable. These packings are differentiated from those occupying the red region, which are heavily overcompressed and are mechanically stable, but additionally have non-zero nullity (are underdetermined with respect to contact forces).

is to attempt to create a tail that exhibits non power-law behavior by sampling force networks non-uniformly, and seeing if the tail exhibits a different length scale. Are there physically realistic sampling biases that could be applied? For instance, it may be that applying a small amount shear to a packing can be captured by a non-uniform sampling of force networks.

## Acknowledgments

This work was supported by NSF-DMR0905880, and has benefited from the facilities and staff of the Yale University High Performance Computing Center and NSF CNS-0821132. We acknowledge useful discussions with S. Franz, G. Biroli, Dapeng Bi, N. Menon and C. S. O’Hern, and with participants at the 2010 Les Houches Winter School. BC acknowledges the Aspen Center for Physics, and the Kavli Institute for Theoretical Physics where some of this work was done.

## References

- [1] AJ Liu and SR Nagel. Nonlinear dynamics - jamming is not just cool any more. *Nature*, 396(6706):21–22, 1998.



- [2] CS O’Hern et al. Jamming at zero temperature and zero applied stress: The epitome of disorder. *Phys. Rev. E*, 68(1, Part 1):011306, 2003.
- [3] C. Heussinger and J-L Barrat. Jamming transition as probed by quasistatic shear flow. *Phys. Rev. Lett.*, 102:218303, 2009.
- [4] Wouter G. Ellenbroek et al. Critical scaling in linear response of frictionless granular packings near jamming. *Phys. Rev. Lett.*, 97(25):258001, 2006.
- [5] M Wyart et al. Effects of compression on the vibrational modes of marginally jammed solids. *Phys. Rev. E*, 72(5, Part 1):051306, 2005.
- [6] AV Tkachenko and TA Witten. Stress propagation through frictionless granular material. *Phys. Rev. E*, 60(1):687–696, 1999.
- [7] M Mailman and B Chakraborty. Signature of a thermodynamic phase transition in jammed granular packings: growing correlations in force space. *Journal of Statistical Mechanics: Theory and Experiment*, 2011(07):L07002, 2011.
- [8] J P Bouchaud and G Biroli. On the adam-gibbs-kirkpatrick-thirumalai-wolynes scenario for the viscosity increase in glasses. *J. Chem. Phys.*, 121(15):7347–7354, 2004.
- [9] G. Biroli et al. Thermodynamic signature of growing amorphous order in glass-forming liquids. *Nature Physics*, 4(10):771–775, 2008.
- [10] Jean Philippe Bouchaud and G. Biroli. Rfot review. *ArXiv:0912.2542*, 2009.
- [11] Andrea Cavagna et al. Mosaic multistate scenario versus one-state description of supercooled liquids. *Phys. Rev. Lett.*, 98(18):187801, 2007.
- [12] Andrea Montanari and Guilhem Semerjian. Rigorous inequalities between length and time scales in glassy systems. *J. Stat. Phys.*, 125(1):22–54, 2006.
- [13] JH Snoeijer et al. Ensemble theory for force networks in hyperstatic granular matter. *Phys. Rev. E*, 70(6, Part 1):061306, 2004.
- [14] Brian P. Tighe et al. The force network ensemble for granular packings. *Soft Matter*, 6(13):2908–2917, 2010.
- [15] S McNamara and H Herrmann. Measurement of indeterminacy in packings of perfectly rigid disks. *Phys. Rev. E*, 70(6, Part 1):061303, 2004.
- [16] JC Maxwell. On the Calculation of the Equilibrium and Stiffness of Frames. *Philosophical Magazine*, 27:294–299, 1864.
- [17] CF Mouzarkel. *Proceedings of Rigidity Theory and Applications Traverse City MI*. Fundamental Material Science Series, Plenum, New York, 1998.
- [18] LE Silbert et al. Vibrations and diverging length scales near the unjamming transition. *Phys. Rev. Lett.*, 95(9):098301, 2005.
- [19] Zorana Zeravcic, Wim van Saarloos, and David R. Nelson. Localization behavior of vibrational modes in granular packings. *EPL (Europhysics Letters)*, 83(4):44001, 2008.
- [20] M Wyart. *On the Rigidity of Amorphous Solid and Price Fluctuations, Conventions and Microstructure of Financial Markets*. PhD thesis, SPEC, CEA Sarclay, Paris, 2005.
- [21] WG Ellenbroek. *Response of Granular Media near the Jamming Transition*. PhD thesis, University of Leiden, 2007.
- [22] Schreck C. F. et al. Jammed particulate systems are inherently nonharmonic. *ArXiv:1012.0369*, 2010.
- [23] C. E. Maloney. Correlations in the elastic response of dense random packings. *Phys. Rev. Lett.*, 97(3), 2006.
- [24] Gregg Lois et al. Stress correlations in granular materials: An entropic formulation. *Phys. Rev. E*, 80:060303 (R), 2009.
- [25] David Chandler and Juan P. Garrahan. Dynamics on the Way to Forming Glass: Bubbles in Space-Time. In *Annual Review of Physical Chemistry, VOL 61*, volume 61 of *Annual Review of Physical Chemistry*, pages 191–217. 2010.
- [26] J. P. Bouchaud. Granular media: some ideas from statistical physics. In J.-L. Barrat, J. Dalibard, M. Feigelman, and J. Kurchan, editors, *Slow Relaxations and Nonequilibrium Dynamics in*

*Condensed Matter*. Springer, Berlin, 2003.

- [27] K. Huang. *Statistical Mechanics, Second Edition*. John Wiley and Sons, New York, 1987.
- [28] BP Tighe et al. Force distributions in a triangular lattice of rigid bars. *Phys. Rev. E*, 72(3, Part 1):031306, 2005.
- [29] SI Newton. *The Mathematical Principles of Natural Philosophy*. Royal Society of London, London, 1687.
- [30] DN Perera and P Harrowell. Stability and structure of a supercooled liquid mixture in two dimensions. *Phys. Rev. E*, 59(5, Part B):5721–5743, 1999.
- [31] RJ Speedy. Glass transition in hard disc mixtures. *Journal of Chem. Phys.*, 110(9):4559–4565, 1999.
- [32] M Dzero et al. Activated events in glasses: The structure of entropic droplets. *Phys. Rev. B*, 72(10):100201, 2005.
- [33] Silke Henkes and Bulbul Chakraborty. Statistical mechanics framework for static granular matter. *Phys. Rev. E*, 79(6, Part 1), 2009.
- [34] Aleksandar Donev, Robert Connelly, Frank H. Stillinger, and Salvatore Torquato. Underconstrained jammed packings of nonspherical hard particles: Ellipses and ellipsoids. *Phys. Rev. E*, 75(5, Part 1), 2007.